https://doi.org/10.1016/j.jechem.2022.12.029
This is the Pre-Published Version.

REVIEW

Recent progress of inverted organic-inorganic halide perovskite solar cells

Dongyang Li[a,b,1], Yulan Huang[b,1], Zhiwei Ren[a], Abbas Amini[e], Aleksandra B. Djurišić[d], Chun Cheng[b,c,*], Gang Li[a,*]

[a] Department of Electronic and Information Engineering Research Institute for Smart Energy (RISE), The Hong Kong Polytechnic University, Hong Kong 999077, China

[b] Department of Materials Science and Engineering, Southern University of Science and Technology, Shenzhen 518055, Guangdong, China

[c] Guangdong Provincial Key Laboratory of Energy Materials for Electric Power, Southern University of Science and Technology, Shenzhen 518055, Guangdong, China

[d] Department of Physics, The University of Hong Kong, Hong Kong 999077, China

[e] Centre for Infrastructure Engineering, Western Sydney University, Penrith 2751, NSW, Australia

* Corresponding authors.

E-mail addresses: chengc@sustech.edu.cn, gang.w.li@polyu.edu.hk

[1] These authors contributed equally to this work.

© 2023. This manuscript version is made available under the CC-BY-NC-ND 4.0 license http://creativecommons.org/licenses/by-nc-nd/4.0/

Dongyang Li is a joint Ph.D. candidate in the in the Department of Electronic Information and Engineering at the Hong Kong Polytechnic University and the Department of Materials Science and Engineering at Southern University of Science and Technology under the supervision of Prof. Gang Li and Prof. Chun Cheng. His research interest mainly focused on perovskite-based optoelectronic materials.

Yulan Huang is a joint Ph.D. candidate in the Department of Materials Science and Engineering at Southern University of Science and Technology and in the Institute of Applied Physics and Materials Engineering at the University of Macau. She received her master's degree from South China Normal University in 2017. Her current research interests focus on organic-inorganic perovskites and their application in solar cells.

Zhiwei Ren is a research assistant professor at the Hong Kong Polytechnic University. He received his Ph.D. degree from the Hong Kong Polytechnic University in 2018, and further worked as the postdoctoral fellow in Nazarbayev University and the Hong Kong Polytechnic University, respectively. His current research interests include perovskite

semiconductors (e.g., solar cells and LEDs), metal oxide nanostructure fabrication and smart flexible electronic devices.

Abbas Amini is an assistant professor at Western Sydney University and Australian College of ACK working on emerging topics in biotechnology, biomedical, nanotechnology, modern materials, nano-energy, and high-tech industries. Dr. Amini has served in academia and industry in Canada and Australia, mostly for the University of Melbourne, Deakin University, Monash University, Western Sydney University, and ACK. He was appointed as the member of the graduation supervision committee (for PhD and MSc candidates) in Western Sydney University from 2014, and currently is an Adjunct Graduation Faculty Member of the University of Toledo, Ohio, USA.

Prof. Aleksandra B. Djurišić obtained Ph. D. degree in Electrical Engineering from the School of Electrical Engineering, the University of Belgrade in 1997. She has been a postdoctoral fellow at the University of Hong Kong and Alexander von Humboldt postdoctoral fellow at TU Dresden. She joined the department of Physics at the University of Hong Kong in 2003 as assistant professor and she is currently a professor. Her research interests include halide perovskite materials, nanomaterials, wide-bandgap semiconductors, and organic materials, and their applications in areas related to energy and environment, such as photocatalysis, solar cells, and LEDs. She has published 392 research articles including reviews, and has been cited over 22000 times. Her h-index is 66.

Chun Cheng received his Ph.D. (2009) in Nano Science and Technology from the Hong Kong University Science & Technology. He did postdoctoral research at the department of physics at Hong Kong University Science & Technology (2009–2011), Berkeley Laurence National Laboratory and the University of California at Berkeley (2011–2013). In 2013, Professor Cheng joined in the department of materials science and engineering of Southern University of Science and Technology as an associate professor. His research interests include smart materials, energy materials, two-dimensional inorganic flexible electronic materials and devices, etc.

Gang Li is Sir Sze-Yuen Chung Endowed Professor in Renewable Energy in the Department of Electronic and Information Engineering, Associate Director of Research Institute of Smart Energy (RISE) in the Hong Kong Polytechnic University. He obtained his B.Sc. degree in Space Physics from Wuhan University (China), M.Sc. in Electrical Engineering, and Ph.D. in Condensed Matter Physics from Iowa State University, respectively. His research interests are materials, device engineering, and device physics in organic semiconductors, and hybrid perovskite semiconductors, focusing on energy applications. He was a postdoc, Research Professor at UCLA, and VP of Solarmer Energy Inc. before coming to Hong Kong in 2016. He has been among Thomson Reuters/Clarivate Analytics Highly Cited Researchers since 2014. He has published ~200 papers, with over 70 000 citations and H-index of 78 (Google Scholar). He is Fellow of Royal Society of Chemistry (RSC), The International Society for Optics and Photonic (SPIE), and Optica (OSA).

Abstract: In recent years, inverted perovskite solar cells (IPSCs) have attracted significant attention due to their low-temperature and cost-effective fabrication processes, hysteresis-free properties, excellent stability, and wide application. The efficiency gap between IPSCs and regular structures has shrunk to less than 1%. Over the past few years, IPSC research has mainly focused on optimizing power conversion efficiency to accelerate the development of IPSCs. This review provides an overview of recent improvements in the efficiency of IPSCs, including interface engineering and novel film production techniques to overcome critical obstacles. Tandem and integrated applications of IPSCs are also summarized. Furthermore, prospects for further development of IPSCs are discussed, including the development of new materials, methods, and device structures for novel IPSCs to meet the requirements of commercialization.

1. Introduction

Solution-processed organic-inorganic halide perovskites (OIHPs) have attracted considerable attention because of their unique optoelectronic characteristics, such as high charge mobility, long carrier lifetime, and high absorption coefficient. To date, perovskite solar cells (PSCs) have achieved a power conversion efficiency (PCE) of 25.7%, which is comparable to the recorded monocrystalline silicon solar cell (~26.1%) and is approaching the Schottky-Queisser limit of single-junction solar cells [1,2]. In 2009, Miyasaka et al. developed organometal trihalide perovskites as sensitizers in the study of dye-sensitized solar cells (DSSCs), which pioneered the use of organometallic halide perovskites in solar cells [3,4].

The structures of PSCs are generally divided into two categories: regular (n-i-p) and inverted (p-i-n) configurations, where the regular can be subdivided into mesoporous (with a mesoporous scaffold) and planar configurations (without a mesoporous scaffold), as shown in Fig. 1(a). The high-efficiency regular PSCs typically utilize spiro-OMeTAD as the hole transport layer, however, this organic material requires complicated doping and oxidation processes, which are less compatible with up-scaling and flexible applications. Compared to PSCs with regular structures, inverted perovskite solar cells (IPSCs) are attractive and may be suitable for flexible, roll-to-roll, and tandem applications [5,6]. Based on the unique photophysical and electrical properties of perovskites, extensive research has been conducted to develop IPSCs. IPSC emerged in 2014 [4,5] using NiO_x or PEDOT:PSS as the hole transport layer (HTL) and PCBM or n-type metal oxides like ZnO as the electron transport layer (ETL) [7–9]. The concept mimics earlier organic photovoltaics (OPVs) with versatile device architectures, where “inverted” OPVs were introduced in 2006 and assisted with the application of p-type metal oxides in OPVs [10,11]. This p-i-n structure has been applied as another type compared to the regular (n-i-p) structure [12–14]. A general structure of IPSCs consists of transparent conductive oxides (ITO)/hole transport layers (HTL)/perovskite active layers (perovskite)/electron transport layers (ETL)/buffer

layers/metal contacts. As shown in Fig. 1(b), IPSCs typically operate as follows: when illuminated by solar irradiation, the active perovskite layer absorbs the photons and generated excitons. These excitons are dissociated into hole-electron pairs, which are further separated and diffused into the transport layer by the built-in electric field. The holes are transferred to the ITO side through the HTL, while the electrons propagate into the metal contacts through the ETL and buffer layer.

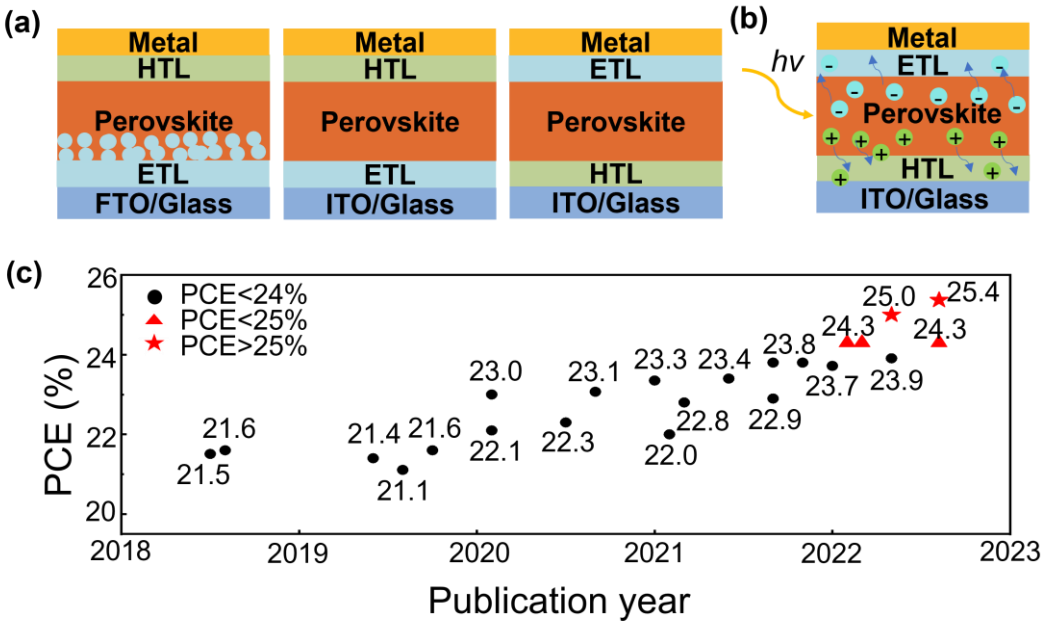

Fig. 1. (a) Typical structures of perovskite solar cells. 1) regular mesoporous, 2) regular planar, 3) inverted planar. (b) Working mechanism of IPSCs. (c) Reported efficiency development of IPSCs in the past 3 years.

The efficiency of IPSC has improved rapidly in recent years, from 21.6% in 2018 to 25% most recently. The reported efficiencies of high-performance IPSCs are shown in Fig. 1(c).[16–38]. Despite this, IPSCs are still less efficient than their regular counterparts. The current gap has been significantly reduced to 1% through surface passivation, but there are still some issues that need to be addressed for further development [30,31]. Herein, we outline recent advances in efficiency of IPSCs . After explaining the working principle and dilemmas of IPSCs, we focus on the interface

engineering and modification of the perovskite layer. In the conclusion section, we discuss recent advances in wide-bandgap and narrow-bandgap solar cells and integrated solar cells with inverted structures.

2. Configuration of IPSCs

2.1 Energy level

Compared to inorganic photovoltaics with large dielectric constants, such as silicon, perovskite photovoltaics are well suited to the free-carrier model, where charges can be easily separated and transported [39]. The typical energy level diagram of IPSCs is shown in Fig. 2(a) [40]. The interfacial energy level affects the dynamics of charge injection and transport. A well-balanced energy level will facilitate charge transfer and extraction, resulting in improved device performance. The charge transport dynamics is related to the highest occupied molecular orbital (HOMO) (or the valence band maximum, VBM) in classical semiconductors and the lowest unoccupied molecular orbital (LUMO) (or the conduction band minimum, CBM) of the device's layers, including ITO, ETL, active perovskite, HTL, and metal contact work function. According to Murata, the mismatch between the band levels should be within 0.2 eV to reduce interfacial loss and obtain high performance. If the energy band is not properly aligned, the energy barrier will increase, resulting in significant energy loss [41,42].

The working principle of IPSCs is illustrated in Fig. 2(b). When the IPSCs are not photoactivated, Fermi-level equilibration/alignment happens in all layers of the device, resulting in an electric field at the interface. When the devices are activated by solar energy entering nonequilibrium conditions, the electrons are excited from the valence band to the conduction band. Then the photogenerated electron-hole pairs are separated into electrons and holes by a built-in electric field. The anode and cathode are responsible for collecting electrons and holes following the diffusion, transport, and extraction processes [43]. Nevertheless, the charges undergo non-radiative recombination due to the bulk or interfacial traps.

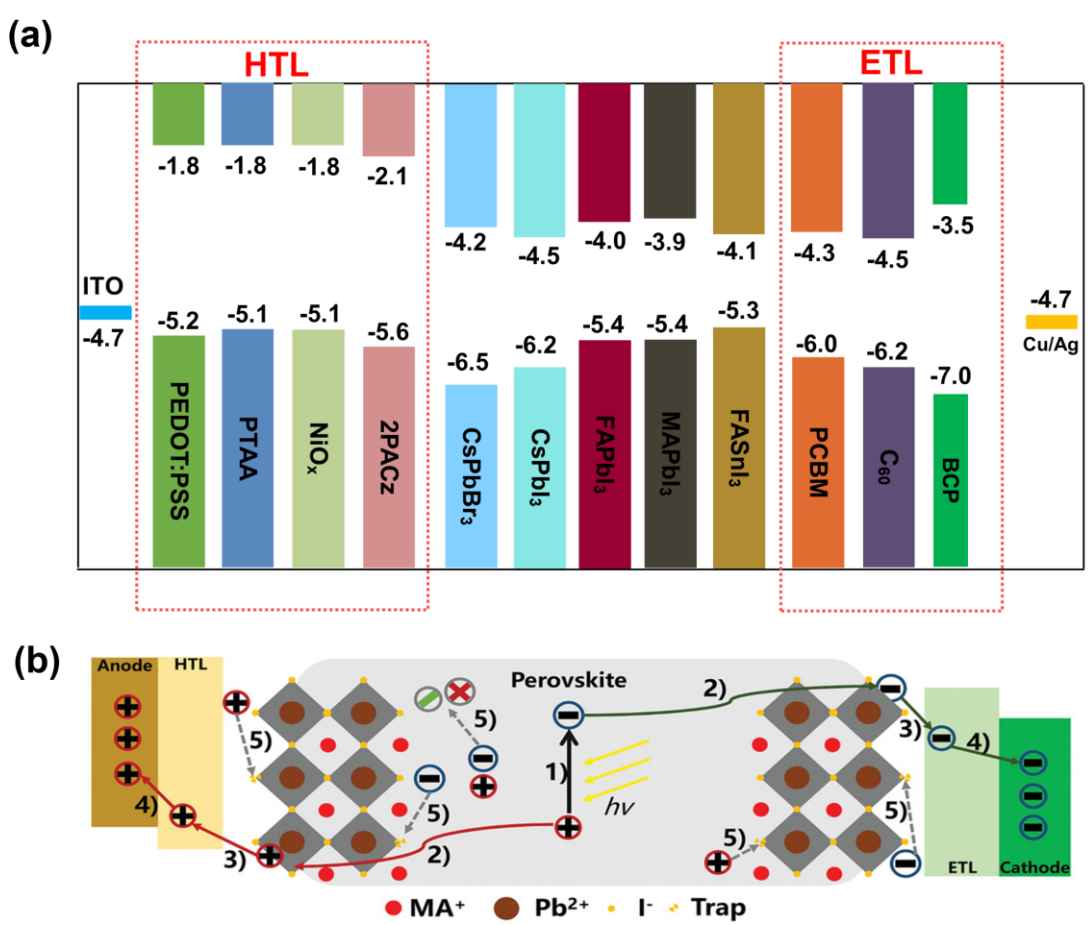

Fig. 2. (a) Scheme of the energy levels of each layer in IPSCs. (b) Working principle of perovskite solar cells: 1) charge dissociation, 2) charge diffusion, 3) charge transport, 4) charge extraction, and 5) charge recombination. Reproduced from Ref. [43] with permission from John Wiley and Sons.

2.2 Defects

The inherent defects in hybrid perovskites induce a significant amount of deep-level traps, which result in nonradiative charge recombination and damage device performance in terms of PCE and stability [44–46]. The trap-assisted recombination in IPSCs can be described by Shockley-Read-Hall (SRH) theory. When defects create deep-level traps, they only trap electrons or holes that cannot escape by thermal activation and then annihilate with oppositely charge carriers [47]. Fig. 3 shows two types of traps in IPSCs, including shallow-level and deep-level traps. Shallow-level traps are originated from point defects such as cation vacancies and halide vacancies

[46]. Both vacancies are not harmful to the performance of perovskite devices and can be re-emitted as charges into CBM or VBM via phonon absorption. However, carrier migration at such point defects can result in unintentional shallow gaps, hysteresis, phase separation, and degradation of IPSCs. Another type of trap, deep-level traps, such as uncoordinated Pb^{2+}, metallic lead clusters, and Pb-I anti-site defects, are deteriorating the performance of photovoltaic devices. The SRH recombination induced by deep-level traps in perovskites is the primary source of charge carrier loss. This phenomenon can be caused by a variety of factors, including the non-stoichiometric ratio of lead iodide and organic cations and the prolonged thermal annealing process [48].

Defects can be located on the surface, at the grain boundaries, or within the grain interiors of IPSCs. Charge extraction and transport are affected by interfacial defects, increasing series resistance and reducing J_{sc} and FF. Defect passivation is considered an effective strategy to reduce non-radiative recombination and suppress ion migration in IPSCs.

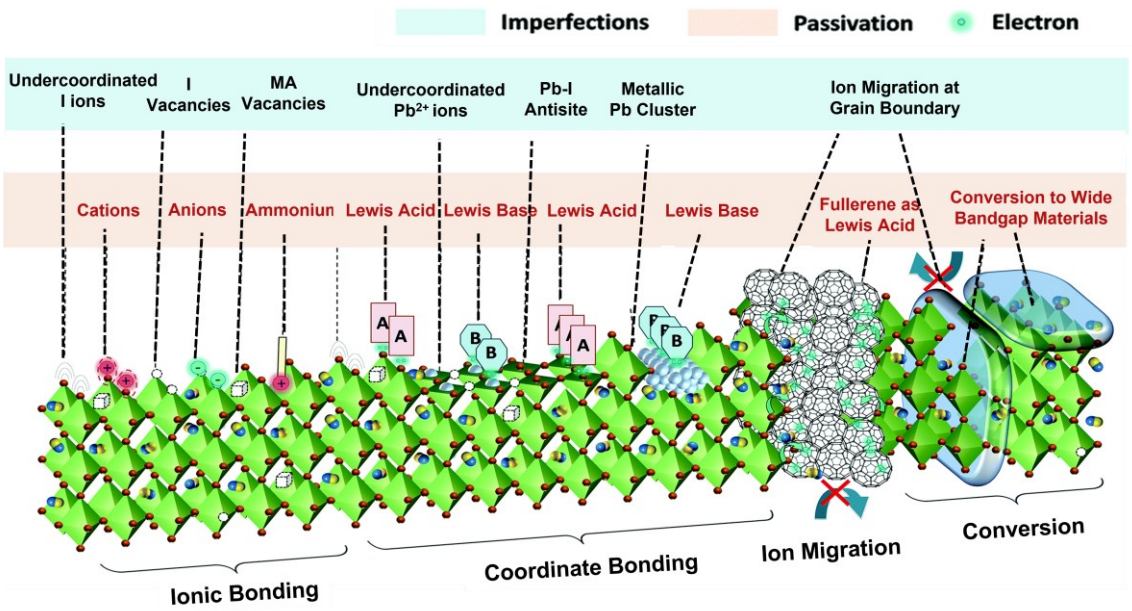

Fig. 3. Imperfections in OIHP film and their passivation strategies. Reproduced from Ref. [46] with permission from the Royal Society of Chemistry.

2.3 Residual strain

Strain-related issues have recently attracted considerable attention because it is a key factor to affect the photovoltaic performance of IPSCs. The strain is generally caused by lattice mismatch during perovskite film growth process and thermal expansion during annealing. The lattice mismatch is due to cage distortions and the PbI_6 octahedral tilt, which is related to the tolerance factor of the perovskite structure. During thermal annealing, the film directly grown on substrates has a low (high) coefficient of thermal expansion compared to perovskite bulk, resulting in tensile (compressible) strains in the planar direction [49,50]. Thermal expansion is one of the primary causes of residual strain in IPSCs.

It is inevitable to prevent the creation of residual strains during the film preparation process. These residual strains can adversely affect perovskite films, especially their efficiency and stability. Bandgap and carrier mobility have been reported to be correlated with strain, carrier extraction, and transport [51,52]. Meanwhile, residual strains bring a concern to the device's stability. Perovskites have been reported to severely degrade to PbI_2 when exposed to illumination or thermal conditions [53,54]. Regulating residual strain has recently emerged as a critical aspect for improving the stability and performance of perovskite-based optoelectronic devices [49–51,55,56].

3. Development of interfacial layer for IPSCs

The inferior performance of IPSCs is primarily due to the sluggish charge extraction and severe non-radiative recombination at the interface, which limit the V_{oc} and FF. The growth of perovskite crystals is highly dependent on the substrate. It is found that perovskites form larger grains on hydrophobic substrates rather than hydrophilic substrates [57]. Furthermore, trap states at the bottom interface of perovskite can result in severe charge accumulation and recombination in IPSCs. Both the crystallization and growth of perovskite grains depend on the bottom interface, and the extraction and transport of holes are also related to the bottom interface. Meanwhile, the top interface plays a crucial role in electron extraction and transport, thus trap passivation and matching energy levels at the perovskite/ETL interfaces should also be systematically investigated [58].

3.1 Bottom interface of IPSCs

A prerequisite for obtaining high-quality perovskite films is to reduce defect density, which significantly depends on the beneath substrate on which the perovskite crystallizes and grows into films. IPSCs cannot be fully optimized without considering the effect of the bottom interface. Perovskite films are affected by the wettability of the substrates used during grain crystallization and growth. Compared to the larger quantity of droplets on hydrophilic substrates, perovskite precursors form relatively few nucleation sites on hydrophobic substrates, such as PTAA, poly-TPD, and some metal oxides [57,59]. Typically, fewer nucleation sites favor the development of larger and high-quality grains. However, non-wetting hydrophobic substrates with poor affinity to the precursor may result in poor continuity and o incomplete coverage of perovskite film with pinholes [60]. Therefore, the quality of perovskite films and device performance can be effectively controlled by manipulating the bottom interface.

3.1.1 PTAA-based IPSCs

PEDOT:PSS was initially used in IPSCs, but the acidity and hydroscopic group were detrimental to the device stability, which resulted in serious degradation of IPSCs. Other p-type organic semiconductor materials are required to be developed as new HTLs. PTAA is currently one of the most promising candidates for IPSCs because it is efficient and stable. Most recent PCEs of PTAA-based IPSCs showed an efficiency over 25% [20,24,31,32,35]. Although PTAA has the potential to have high efficiency and stability, there is an excessive amount of small-sized crystals that resulted in high trap density at the interface between PTAA and perovskites [61]. A slight mismatch in energy levels between the HOMO of PTAA and the VBM of perovskite also brings unfavorable energy losses at the interface [62].

The modification of PTAA by surface treatment is considered an effective method to improve the performance of devices. It is worthwhile to investigate the PTAA/perovskite interface to improve the quality of perovskite films in IPSCs [63,64]. Recently, Neher and Zhang adopted a conjugated polyelectrolyte (PFN-Br) as an interfacial layer for both PTAA and poly-TPD [17,65]. The PFN-Br plays several functions. First, the incorporation of PFN-Br is suggested to improve the wettability and surface energy of PTAA substrate by the polar quaternary ammonium group. Second, the quaternary group tends to interact with $[PbX_6]^{4-}$ octahedral via electrostatic interaction. Finally, the Br groups in PFN-Br can passivate the halide vacancy, resulting in high-quality perovskite film with reduced defects [66–68]. Combined with a LiF treatment at the perovskite/ETL interface, the non-radiative recombination loss was suppressed at both interfaces, resulting in higher V_{oc} and FF. Similarly, Zhang and co-workers proposed the use of 3-(1-pyridinio)-1-propane sulfonate (PPS) as a chemical bridge at the PTAA/perovskite interface [69]. The PPS molecule with the functional pyridine group is expected to passivate the interfacial defects and suppress non-radiative recombination. Meanwhile, the S=O bond in PPS exhibits strong coordination with the empty orbital of Pb^{2+} in the perovskite. As a further illustration of the passivation properties of PPS molecules, Fig. 4(a) shows the charge collection and

recombination scheme at the two interfaces. The molecular can be used to reduce the density of traps in perovskites by passivating halide and cation vacancies. Also, PPS can adapt PTAA to achieve a more favorable energy alignment within IPSCs, facilitating hole extraction and carrier transfer at the interface.

In addition to the interface engineering of PTAA, the target design of new PTAA molecules with functional groups has been reported to enhance wettability, build deeper energy levels, and passivate interfacial traps [70]. Gao et al. introduced polar methoxy groups into the para and ortho positions of the dangling benzene in the PTAA molecular structure and produced 2MeO-PTAA [71]. Asymmetric methoxy groups with electron-donating properties increase the surface energy, facilitating tight interfacial contacts and hole extraction at the PTAA/perovskite interface. The PCE and FF of the 2MeO-PTAA-based device increased to 20.23% and 0.84 with negligible hysteresis, which is possibly due to decreased surface defects and reduced shunt resistance losses. Similarly, Wu et al. substituted the alkyl groups in PTAA with multifunctional pyridine groups to change the ortho- (o-PY), meta- (m-PY) linking site of the pyridine unit to para-location (p-PY); this modification improved the performance of IPSCs [72]. In addition to the hydrophilicity, the passivation efficacy was enhanced using the pyridine functionalized PTAA. It showed 22% efficiency for a small-size device (0.09 cm^2) and 20% for an upscaled device (1 cm^2).

3.1.2 NiO_x-based IPSCs

Organic HTMs suffer from the high cost of their raw materials, the drawback of upscaling fabrication, and undesirable thermal stability; these restrict the application and commercialization of IPSCs. Alternatively, inorganic p-type metal compounds with high transparency, such as cooper families (Cu_2O, CuSCN, CuI, $CuGaO_3$), molybdenum oxide (MoO_3), vanadium oxide (VO_x), and nickel oxides (NiO_x) have attracted much attention [13,75]. Among them, NiO_x has attracted extensive attention because of its suitable work function, high transmittance, and high thermal/light

stability. However, NiO_x HTLs have unsatisfactory conductivity and a large number of surface defects, which would cause severe interfacial charge recombination, resulting in poor V_{oc} and FF [76].

Various strategies, such as metal doping and surface treatment, have been employed to optimize the performance and reduce the energy loss of NiO_x-based IPSCs. Intrinsic NiO with stoichiometric Ni^{2+} and O^{2-} is insulation; it always requires self-doping of Ni^{3+} to construct p-type NiO_x. However, the considerable ionization energy of Ni^{3+} hinders the conductivity, thus limiting the application of NiO_x. In this regard, universal doping strategies have been proposed to optimize the energy structure and conductivity [77–79]. Liu et al. synthesized Samarium-doped nickel oxide (Sm:NiO_x) using a facile chemical precipitation method [80]. It is suggested that the Sm^{3+} doping can reduce the formation energy of Ni vacancy and increase the density of Ni vacancies, therefore increasing the hole density. Consequently, IPSC based on Sm:NiO_x HTL delivers a champion efficiency of 20.71%, which is ascribed to the enhanced conductivity and work function. More importantly, Sm:NiO_x is also compatible with larger-area applications, which delivers PCE of 18.51% (area 1 cm^2) and 15.27% (16 cm^2). Another ionic liquid-assisted synthesis strategy (NiO_x-IL) was recently proposed by Li et al. by adding 1-butyl-3-methylimidazolium tetrafluoroborate ([BMIm]BF_4) into $Ni(NO_3)_2$ precursor; the synthesis scheme is illustrated in Fig. 4(b) [73]. It is illustrated that $[BMIm]^+$ cation had lower adsorption energy than NO_3^- to be adsorbed with $Ni(OH)_2$ via hydrogen bonding in the precursor solution. This setup effectively increased the conductivity of as-prepared NiO_x-IL films and suppressed the redox reaction in the buried NiO_x-IL/perovskite interface. The energy band diagram of NiO_x-IL-based devices has been alleviated by downshifting closer to the valance band of perovskite, where the hole transfer and injection are improved at the NiO_x-IL/perovskite interface. As a result, the NiO_x-IL-based IPSCs delivered an efficiency as high as 22.62% with superior stability, which maintained 92% of its initial value under maximum power point tracking and 1000-hour sun illumination.

Surface treatment by inorganic and organic materials is denoted as another effective strategy to improve the conductivity and optimize interfacial defects of NiO_x [81–83]. Recently, Chang et al. recently adopted CsBr as an interfacial buffer layer between NiO_x and perovskite layer [84]. Confirming by the XRD results, it is demonstrated that the smaller Young's modulus of CsBr (16.2 GPa) is expected to reduce the lattice strain of initial perovskite (17.8 GPa) under the thermal annealing process. Consequently, IPSCs with the relieved perovskite lattice strain and reduced interface traps delivered an efficiency of up to 19.7%. In addition, Chen and colleagues developed a series of molecules, including TCNQ, F2TCNQ, F4TCNQ, and F2HCNQ on the NiO_x/perovskite interface to control the electron affinity [22]. It was found that the conductivity of NiO_x is improved more than tenfold after the introduction of F2HCNQ, which could be resulted from the deeper LUMO and increased hole concentration in the VB. Moreover, the energy gap between E_F and VB is decreased from 0.5 eV (control) to 0.24 eV (F2HCNQ), resulting in fast hole extraction with lower interfacial energy loss. This method drastically enhanced the V_{oc} and FF of IPSCs, which obtained the PCEs of 22.13% for small rigid (0.09 cm^2) and 12.85% for the flexible mini-module (36.1 cm^2).

Sargent et al. recently modified the surface of NiO_x using organic spacer cations with -NH_2-rich groups such as n-butylammonium (BA), ethylammonium (EA), dimethylammonium (DMA), guanidinium (GUA) [28]. It is proved that the highly symmetric structure of GUA and -NH_2 functional groups have a large binding affinity to O atoms on the NiO_x surface via hydrogen bonding (Fig. 4c); this induces the formation of 2D perovskite at the buried interface. The 2D perovskite can act as both seeds for perovskite crystallization and passivation layer for reducing defect density. As a result, the wide-bandgap (1.7 eV) device based on GUAI seeds showed a champion PCE of 20.1%. Meanwhile, the method could be compatible with 1.55-eV bandgap perovskite system, which yielded an efficiency of up to 22.9%, a milestone among the highest efficiency of NiO_x-based IPSCs.

Inspired by regular mesoporous structure, NiO_x with mesoporous scaffold has also attracted the attention of researchers. The mesoporous structure can provide light management and increase the contact area of HTM/perovskite for efficient hole extraction and transport. There are desirable candidates of mesoporous scaffold for IPSCs such as NiO_x [85,86], Al_2O_3 [87] and $CuGaO_2$ [74–76,88]. Zhang et al. proposed a mesoporous $CuGaO_2$ as mesoporous layer for IPSCs [74]. The mesoporous $CuGaO_2$ severs as a perovskite scaffold, enabling increased light absorption due to light scattering and reduced reflection in the device. In addition, the graded energy alignment shows superior charge transfer and collection at the NiO_x/perovskite interface. Furthermore, they later reported that the performance of mesoporous $CuGaO_2$ could be further increased by doping Zn^{2+} [88]. These advantages of mesoporous $CuGaO_2$ enabled high efficiency and superior stability compared to planar NiO_x IPSCs. Similarly, the utilization of mesoporous NiO_x (mp-NiO_x) was employed via triblock copolymer template-assisted strategy by Tress et al. [85]. The mp-NiO_x-based IPSCs delivered a higher J_{sc} of 23.8 mA/cm^2 compared to 22.9 mA/cm^2 for planar NiO_x devices, which could be ascribed to the enhanced light trapping and absorption in the adjacent perovskite film in the mp-NiO_x structure.

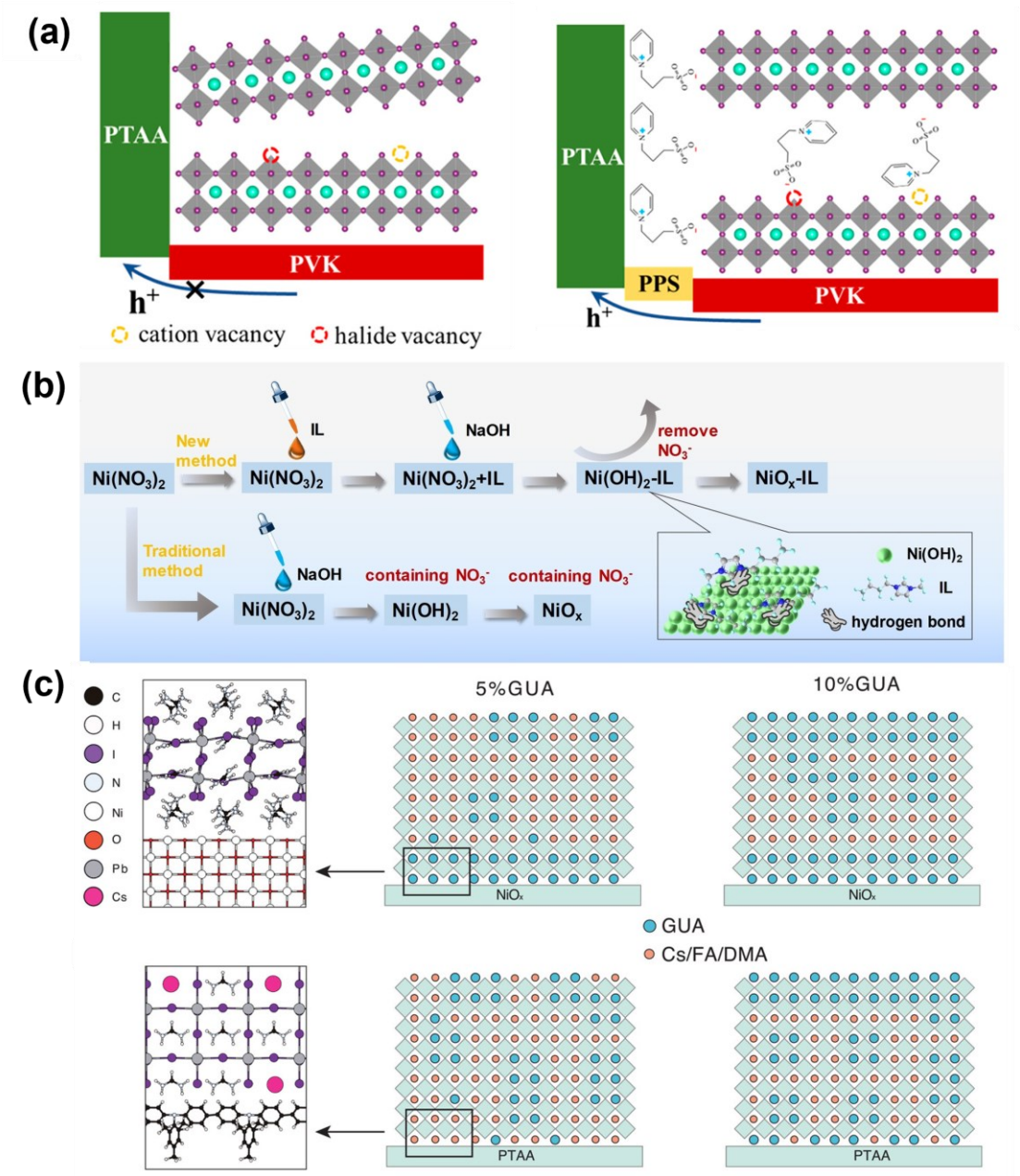

Fig. 4. (a) Schematic illustrations of charge transport between PTAA and perovskite with/without PPS. Reproduced from Ref. [69] with permission from the American Chemical Society. (b) Scheme of synthesis of NiO_x and NiO_x-IL nanoparticles. Reproduced from Ref. [73] with permission from John Wiley and Sons. (c) Mechanism of GUA_2PbI_4 interaction with NiO_x and PTAA substrate. Reproduced from Ref. [28] with permission from John Wiley and Sons.

3.1.3 SAMs-based IPSCs

Self-assemble monolayers (SAMs) contain organic molecules that are anchored as a monolayer to substrates (typically metals and metal oxides) via chemical bonds. SAMs can be tailored to fulfil the intermolecular interaction with high affinity to the substrates. SAMs can be attached to the surface by simple spin-coating or dip-coating methods to form extremely thin and stable layers. Moreover, the optoelectrical properties of SAMs, such as conductivity and work function, can be tuned by functionalization of different groups. These SAMs are currently regarded as novel HTL candidates for IPSCs with high efficiency and high stability. In IPSCs, SAMs of organic molecules on the ITO surface are usually denoted as conventional single-atom HTL to facilitate hole injection at the ITO side [89,90,91]. The use of carbazole bodies with phosphonic acid groups (2PACz, MeO-2PACz and V1036) was firstly reported as SAMs for IPSCs by Albrecht and co-workers [92]. As shown in Fig. 5(a), the 2PACz and MeO-2PACz are expected to form strong bonds with ITO to provide deeper work function SAMs. From the band edge positions shown in Fig. 5(a), it is demonstrated that the HOMO of 2PACz is closest to the VBM of perovskite, which is beneficial to hole extraction and transport. Moreover, they conducted ultraviolet photoelectron spectroscopy (UPS) and photoluminescence (PL) measurements to further verify the minimized interfacial recombination and extended carrier lifetime of perovskite on 2PACz. As a result, the 2PACz-based IPSCs delivered a PCE of 20.9% with a high V_{oc} of 1.19 V. The most important reason for the improved performance can be derived from the surface dipole and shifted vacuum level of ITO coated with SAMs such as 2PACz and MeO-2PACz [91]. To date, 2PACz and MeO-2PACz-based IPSCs have been reported to be among the most efficient IPSCs, with the efficiency exceeding 24% and 25% [33,37]. Hereafter, they designed a novel SAM with methyl group ([4-(3,6-dimethyl-9H-carbazol-9-yl)butyl]phosphonic acid, Me-4PACz) [93]. The Me-4PACz enabled fast hole extraction with reduced phase segregation for wide bandgap (1.68 eV) IPSCs. The ultra-thin SAM (<1 nm) with high conductivity was also found to reduce the transport loss, resulting in a PCE of >20% and an ultra-high FF of 0.84 for wide-

bandgap IPSCs. The fast hole extraction property of Me-4PACz could be transferred to monolithic tandem solar cells, which enabled the perovskite/Si tandem to obtain a high efficiency of >29% and superior operational stability. Most recently, Hong's group reported a series of halogenated phenothiazine-based SAMs [94,95]. As shown in Fig. 5(b), the SAMs containing O, S, or Se heteroatoms can interact with perovskite absorber with increasing order of Se > S > O. In fact, the increased interaction energy reduces the interfacial trap density and increases in the lifetime of charge carrier at the SAM/perovskite interface. These resulted in maximum PCEs of 22.73% (Br-2EPSe), 21.63% (Br-2EPT), and 21.02% (Br-2EPO) for SAM-based PSCs, respectively.

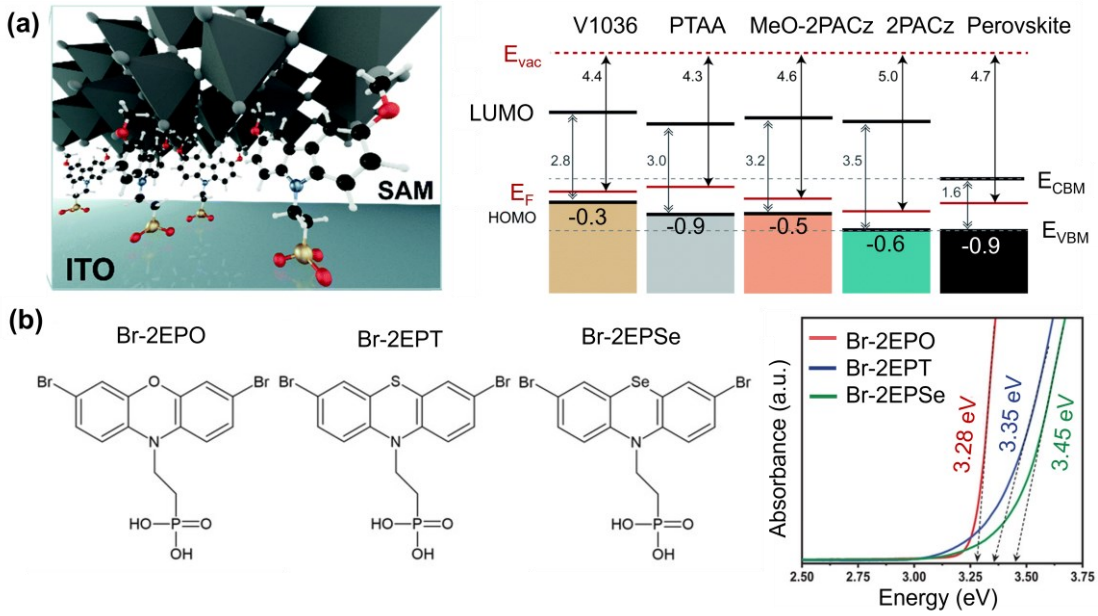

Fig. 5. (a) Schematic demonstration and energy level alignment of SAM HTL and perovskite in the SAM-based IPSCs. Reproduced from Ref. [92] with permission from the Royal Society of Chemistry. (b) Molecular structures and UV-vis absorption spectra of the Br-2EPO, Br-2EPT and Br-2EPSe. Reproduced from Ref. [94,95] with permission from John Wiley and Sons.

3.1.4 Characterizations of buried interface and addressing the stability of IPSCs

The buried interface is the interface that is in direct contact with the bottom of the

perovskite film. This property of the buried interface in IPSCs makes it difficult to characterize and thus has been a challenging research topic. In addition, the sequential spin-coating deposition of perovskite films involves perovskite formation, ink formulation, crystal nucleation and growth, morphology, and defects formation, posing more challenges to the way of studying the buried interfaces [2,96–98]. Due to its non-exposed nature, the fundamental properties of buried interfaces are very difficult to investigate directly. Researchers have largely ignored the direct characterization of charge accumulation at the deep-level traps on the buried interface, which causes non-radiative recombination and limits the device performance. Jen et al. used large alkylammonium interlayers to modify the buried interface, such as phenylethylammonium iodide (PEAI), 1,4-butanediammonium iodide (BDAI), and guanidinium iodide (GAI), which suppress interface recombination and reduce trap states at the PTAA/perovskite interface.[25] As illustrated in Fig. 6(a), the GIWAXS images show that the diffraction rings of LAIs-based perovskite films are sharper and brighter than those of control films, indicating that LAIs modified PTAA can enhance the crystallinity of perovskite films. As a result, high efficiency of 22.3%, with BDAI as the bottom interlayer between PTAA and perovskite, has been achieved. Due to the limitations of characterization technologies, however, a comprehensive analysis of the buried interface has not been conducted.

Impressively, several methods have been applied to solve this dilemma. For instance, Zhu and colleagues reported a lift-off method that uses orthogonal solvents for the PTAA (CB) and perovskite precursor (DMF/DMSO) where the as-prepared perovskite films cannot be dissolved in CB. Upon immersing the quasi-PSC device into CB solution, the as-formed PTAA layer can be re-dissolved and the perovskite films can be lifted-off without any change in the structure, morphology and polycrystalline features. The lift-off stage is illustrated in Fig. 6(c) [99]. In this study, they observed that the recombination loss is originated from sub-microscale imperfections and inhomogeneities at the buried interfaces. Besides, the bright grains composed of PbI_2

and $PbBr_2$ are distributed throughout the perovskite film, with smaller grains near the top surface and larger grains near the buried interface. Moreover, the buried interface displays lower PL intensity with the presence of lead halides, which is due to the annihilation of the photo-generated charge carriers. Similar to dissolution of PTAA in CB, Huang and co-workers developed another approach by using epoxy and cover glass taped with perovskite to mechanically peel off the PTAA/ITO substrate; this method is illustrated in Fig. 6(d) [100]. They revealed that the polycrystalline perovskite films fabricated by one-step spin-coating and blade-coating possessed a downward grain growth direction. This phenomenon is less sensitive to the wettability of substrates or the compositions of perovskites due to the escape of residual solvent.

Removing detrimental lead halides is vital to the efficient operation of devices. Chen et al. further developed phenylethylammonium iodide (PEAI), aminoethylpyridineiodide (AEPI), and phenyldimethylammonium iodide ($PDMAI_2$) as 2D spacers in the buried interface [101]. Combining the lift-off method with 2D spacers, they found that the 2D spacers at the bottom tended to form 2D perovskite structures, indicating that a major amount of 2D spacers would remain and form 2D/3D perovskite heterojunction. With the APEI modification, the VBM of the bottom of the perovskite shifts upward from −5.58 eV (control) to −5.51 eV (AEPI modification). The 2D/3D heterojunctions were induced due to the distribution of the 2D perovskite upon formation, which facilitated hole transfer and suppressed interfacial charge recombination. Most recently, Zhang et al reported ion compensation of pre-buried interfaces for mesoporous IPSCs [102]. FAI solution treatment effectively compensated I^- ion vacancy and regulated the interfacial band energy. This ion compensation strategy could not only repair the ion loss in-situ and improve the built-in electric field, but it also lowered the charge injection barrier and suppressed the interfacial recombination. Owing to these merits, the resultant Cs/FA-based IPSCs demonstrated a PCE of 22.42% and excellent thermal and light stability, and a high PCE (23.11%) was obtained for the CsFAMA triple-cation IPSCs. Except for 2D spacers, most recently, a zeolitic

imidazolate framework (ZIF-6) containing metal and organic functional groups was applied to the buried interface between perovskite and PTAA [98]. The N atoms of ZIF-67 serve as an anchor point for the uncoordinated Pb^{2+} in perovskite, in which the Co element in ZIF-67 is simultaneously coordinated with the N atoms of PTAA. The flexible IPSCs with ZIF-67 were able to offer a high efficiency of up to 20.2% due to the reduced energy level (Fig. 6b). Notably, the flexible device exhibited a long lifespan and remained 78% of its initial PCE after 10000 cycles.

Stability is one of the most important factors for the commercialization of perovskite photovoltaics. IPSCs show excellent stability due to the elimination of ion-doped HTLs commonly used in regular devices. The recent development of operational stability of IPSCs with different HTLs is summarized in Fig. 6(e) [32,33,35–37,73,98,102–114]. The best PTAA-based IPSCs delivered an ultra-high efficiency of >25% with less than a 2% efficiency drop after continuous illumination for 1500 h [35]. It is also noteworthy that the champion devices based PTAA HTL have passed the dame-heat test (85 °C and 85% RH, IEC61215:2016 qualification) with a T_{95} over 1000 h. For NiO_x-based IPSCs, the unencapsulated IPSCs (champion PCE of 23.91%) showed no degradation but 4.9% overflowing of PCE after MPP tracking for 1000 h with the ISOS-L-1I qualification [36]. Moreover, the novel SAM-based IPSCs also delivered satisfied operation stability, the best device retained more than 85% of the initial PCE after 2482 h illumination [37].

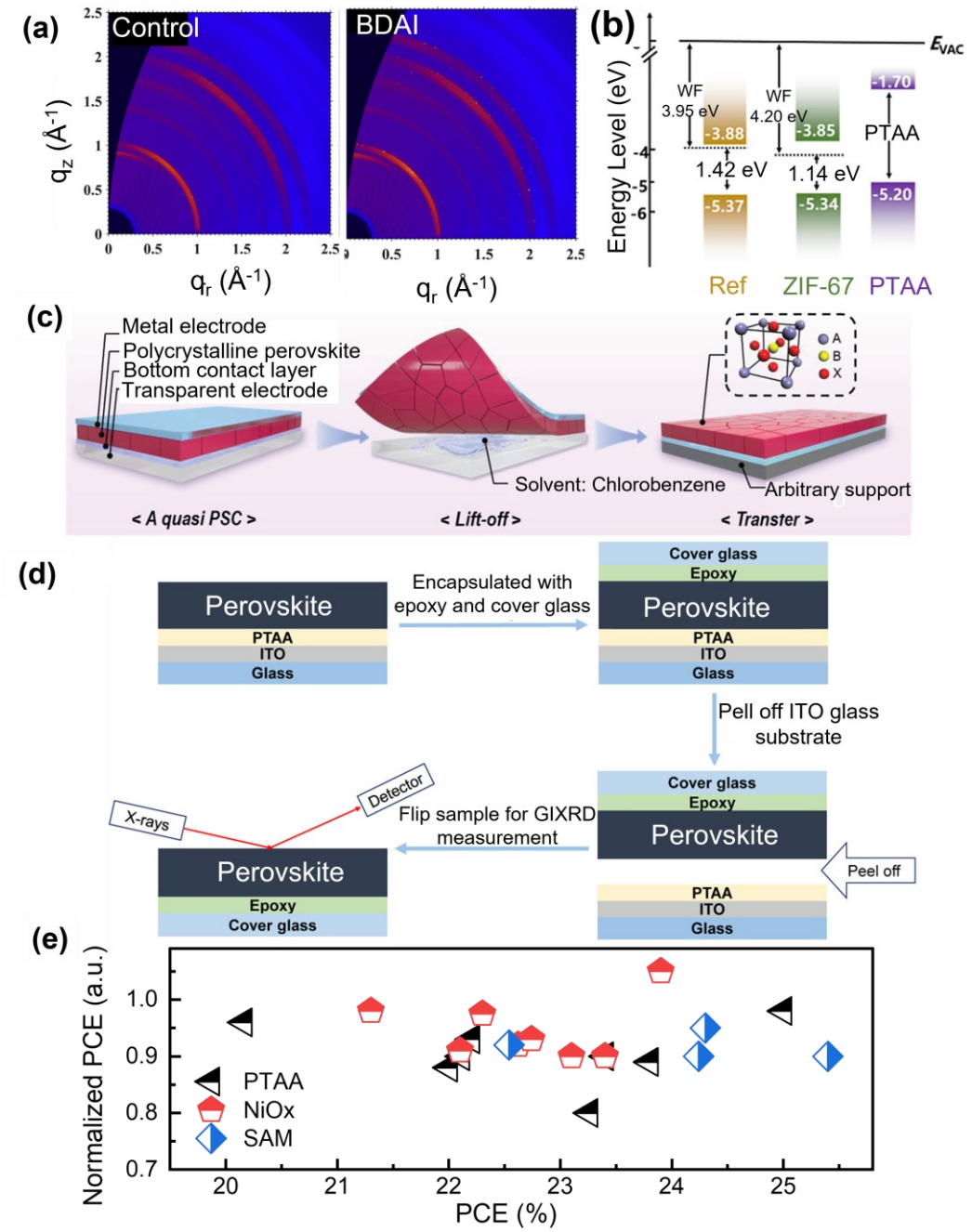

Fig. 6. (a) GIWAXS patterns of control film and perovskite film with BDAI. Reproduced from Ref. [25] with permission from Elsevier. (b) The energy level of IPSCs with ZIF-67. Reproduced from Ref. [98] with permission from Elsevier. (c) Schematic illustration of the lift-off process. Reproduced from Ref. [99] with permission from John Wiley and Sons. (d) Schematic illustration of mechanical peel-off process. Reproduced from Ref. [100] with permission from the American Association for the Advancement of Science. (e) Recent development of the stability of IPSCs based on the selected HTLs under MPP for about 1000 h.

3.2 Top surface of IPSCs

The top surface of perovskite is responsible for electron extraction and hole blocking in IPSCs. Similar to traditional inorganic semiconductors, e.g., silicon and GaAs, surface passivation is an effective way to migrate perovskite's surface defects. This strategy is more efficient for organic-inorganic halide perovskites, as the trap types and distributions are complex. Surface charge trap sites, such as undercoordinated Pb or halide vacancies, are detrimental to the performance and stability of perovskite devices. Numerous approaches, such as surface passivation using organic and inorganic materials, are applied to reduce surface recombination and match surface energy level and passivate the surface defects.

3.2.1 Construction of LD/3D perovskite heterojunction

Organic salts are regarded as efficient passivation agents for IPSCs. Organic spacers tend to form low-dimension (LD) perovskite and construct LD/3D heterojunction at the top surface of perovskite. Suppressing the non-radiative recombination loss by surface passivation with organic materials, such as organic salts and polymers, has been devoted to improving the performance of IPSCs [16,20,21,33,96,108,115–121]. Bifunctional molecules like Piperazinium iodide (PI) and piperazinium diiodide (PDI) are also introduced to the top surface of perovskite [21]. As shown in Fig. 7(a), compared with two $R_2NH_2^+$ groups in the PDI molecule, the PI molecule contains one R_2NH group and one $R_2NH_2^+$ group in the same six-membered ring, which can act as both an electron donor to passivate undercoordinated Pb^{2+} and an electron acceptor to react with the FA^+/MA^+ vacancies. Meanwhile, the residual strains of control, PDI-perovskite and PD-perovskite are systematically investigated through the grazing incidence X-ray diffraction (GIXRD) measurement. It is demonstrated that the scattering peaks gradually shift to the left by varying φ from 10° to 60° at different levels; this indicates the existence of tensile stress at the perovskite film. The residual strain can be released after the surface treatment,

decreasing from 61.57 ± 6.92 MPa for the control film to 27.54 ± 2.16 and 40.15 ± 3.89 MPa for PI and PDI-based perovskite films, respectively. Moreover, after coating PI on the perovskite surface, the VBM and E_F shift 180 meV and 350 meV towards the vacuum. This observation indicates better energy level alignment and improves electron transfer, thus resulting in an enhanced PCE (23.37%). Recently, it was reported that growing 2D perovskite layers on the top surface of 3D perovskite to form 2D/3D junctions could effectively passivate surface trap states and inhibit ion migration among the devices [122]. However, this strategy was more suitable for regular structured PSCs where the 2D perovskite layer is inserted between the 3D perovskite layer and HTL; the try failed for the ETL side of IPSCs. Wolf's group reported an ultra-high efficiency of IPSCs using oleylammonium-iodide (OLAI) molecules [33]. They found that the passivation of the 2D perovskite could compensate the weak passivation property of fullerene through tuning the dimension (*n* value) of the 2D perovskite in the IPSC. Indeed, the post treatment of 2D perovskite tends to form low-dimensionality (n=1) after thermal annealing (2D-TA). However, higher dimensionality ($n\geq2$) could become more pronounced when the post treatment with OLAI molecule was performed at room temperature (2D-RT) (Fig. 7b). As expected, the 2D-TA films were dominated by low dimension (n=1) layers in GIWAXS results. In contrast, the 2D-RT films exhibited diffraction peaks at n=1 and 2, with the n=2 peak being more prominent. Cross-sectional HR-TEM images also showed the existence of n=1 and 2 layers in 2D-RT samples Fig. 7(c). Meanwhile, compared to higher CBM of 2D-TA perovskite, the 2D-RT perovskite film showed closer CBM to the C_{60}, resulting in more efficient charge transfer between the 2D/3D perovskite and C_{60} interface (Fig. 7d). The 2D-RT-based IPSCs showed a substantially improved PCE of 24.3% with an ultra-low V_{oc} deficit of 0.34 eV. Besides, the 2D-RT-based IPSCs exhibited high stability, passing the industry-relevant damp test after 1000 h. Furthermore, quasi-2D surface treatment was also conducted by Sargent and colleagues, who verified that a capping layer with $n\geq3$ 2D ligands could reduce resistance and carrier transport, which was also beneficial for an

inverted structure. But for 2D layer with n=1, the unfavorable energy level alignment would lead to inferior device performance [36,123].

Among the various strategies that have been applied to reduce nonradiative recombination losses in IPSCs, dual passivation of additives, especially double-side treatment using long-chain alkylammonium salts, are suggested to be one of the most effective passivation methods for efficient IPSCs [124]. Paetzold et al. [125] used a long-chain alkylammonium salt phenethylammonium chloride (PEACl), as addictive (grain boundary passivation, GBP), surface passivation (surface passivation, SP) and simultaneous GBP&SP treatment. After the latter treatment, the PEACl could simultaneously passivate the grain boundaries and perovskite/C_{60} interfaces. The energy band diagrams of SP, GBP and GBP&SP-treated perovskites showed a more n-type property, specifically GBP&SP treatment. The GSP-treated device showed an enhancement of 26 mV in V_{oc}, whereas the SP-treated device exhibited a significant improvement in both V_{oc} (1.09 V to 1.13 V) and FF (0.79 to 0.82), resulting effective defect passivation. Upon the dual passivation via GBP&SP treatment, the device performance increased to 22.7%. Owing to the improved electron mobility, reduced trap density, and optimized energy level structure by PEACl treatment, the GBP&SP device obtained the highest efficiency of MA-free IPSC to date. In another study, double-side treatment of the perovskite layer with PEAI was proved to be an efficient method for improving the HTL/perovskite and ETL/perovskite interfaces [31]. First, modifying the buried interface could form a uniform film without nanovoids. In addition, top surface modification effectively passivates the defects and alleviates the energy alignment in the perovskite/ETL; this setup improves electron extraction and reduces interfacial recombination. As a result, J_{sc}, FF and V_{oc} are improved, reaching a prominent PCE as high as 23.7%.

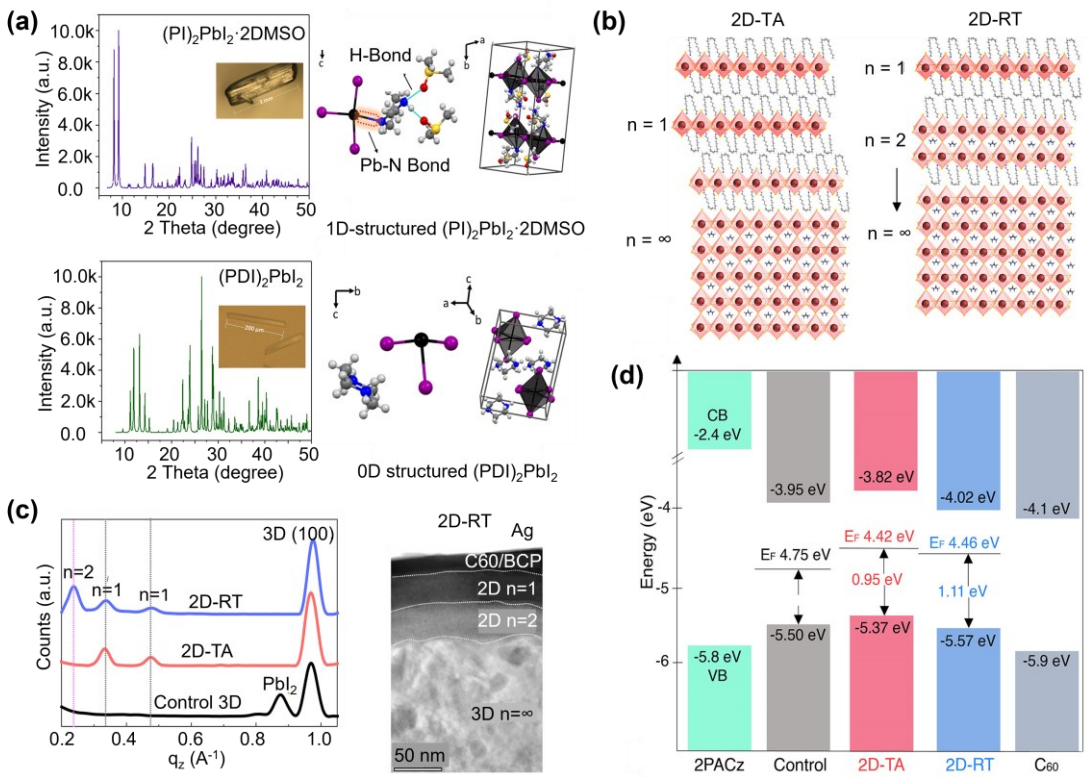

Fig. 7. (a) XRD patterns and structural images of LD perovskite single crystals. Reproduced from Ref. [21] with permission from the American Chemical Society. (b) Scheme of 2D passivation with varied *n* layers under annealing and room temperature. (c) Integrated GIWAXS maps and cross-sectional HR-STEM image. (d) Energy level scheme. Reproduced from Ref. [33] with permission from the American Association for the Advancement of Science.

3.2.2 Organic bonding for surface treatment

Another efficient strategy is to introduce organic materials, including polymers and organic salts, into antisolvents in the one-step spin-coating process. This facile method without additional post treatment has attracted much attention in PSC fields [113,119,126–130]. An ultra-high FF of 0.86 can be obtained by incorporating a novel polymer (PPP) with a 3D star-shape into CB antisolvent [113]. The 3D PPP molecule has multiple chemical anchor joints with perovskite, including the interaction of C═O with PbI_2 and hydrogen bonding between -CF_3 and FA^+/MA^+ of the perovskite (Fig.

8a). In addition, the PPP molecular existing in the grain boundaries of perovskite can also regulate the crystallization of perovskite films, contributing to the regular vertical and dense arrangement of larger grains. The PPP-based PSCs deliver an improved PCE (22.1%) with an ultra-high FF (0.86). The increased FF value, approaching the S-Q limit (0.904) of single-junction solar cells, originates from the increased carrier mobility (Fig. 8b). Star-shaped polyhedral oligomeric silsesquioxane-poly(methyl methacrylate) polymer (POSP) was also developed as an interfacial modification for IPSCs [108]. POSP is suggested to induce a POSP-CsFAMA intermediate phase with perovskite, mainly due to the strong bonding of C=O in the POSP polymer with the Pb^{2+} in perovskite. The intermediate phase causes the crystal growth rate to slow down. This phenomenon randomly forms the nuclei to regulate the growth orientation and minimize the Gibbs free energy in the thermal annealing process, thereby enlarging the grain sizes and reducing trap states. Moreover, the operational stability of PSOP-modified perovskite is impressively improved, with T80 (time to retain 80% of the initial efficiency) over 3982 h. Introducing organic salts, e.g., MA^{+}/FA^{+}, into the antisolvent is another effective strategy to re-regulate the perovskite grain growth and crystallization. However, the poor solubility of these organic salts in common non-polar antisolvent, such as chlorobenzene (CB), diethyl ether (DE) and ethyl acetate (EA), obstructs the development of PSCs. Fortunately, polar solvents, such as isopropyl alcohol (IPA) and ethanol (EtOH), were found to be efficient as antisolvents for PSCs as well [131]. There are some challenges that still need to be addressed, for example, the use of ethanol as an antisolvent can partially decompose the perovskite surface and lead to ununiform and low-quality perovskite film. Besides, high polarity and low boiling point of ethanol contribute to unfavorable trap-rich perovskite surfaces. More recently, Wei and co-workers adopted methylamine bromide (MABr) into ethanol antisolvent as an additive to solve these hurdles [126]. On the one hand, MABr is suggested to compensate the vacancy of organic salts (FAI) during the reaction and decomposition processes. As shown in Fig. 8(c), ethanol-perovskite thin films exhibited

a network of layered crystals with sizes ranging from 100 to 400 nm and many surface pinholes. Upon the addition of 1 mg/mL MABr into ethanol, the crystal size is increased and the pinholes are significantly reduced. Once the MABr concentration is increased to 2 mg/mL, the perovskite film shows high quality without defects and larger crystal sizes of up to 500 nm; this facilitates the charge carrier transport by suppressing carrier recombination. However, needle-like crystals are seen with an increased density of up to 5 mg/mL; the insulating properties tend to impede carrier transport. Fig. 8(d) shows the transient absorption spectra (TAS), which verify the lower density of surface defects after passivation by MABr. The TAS result is direct evidence for the inhibition of nonradiative recombination by incorporating MABr into ethanol as an antisolvent to fabricate perovskite films. As a result, the incorporation of MABr can improve the device performance through improved high-quality perovskite films and reduced non-radiative recombination loss.

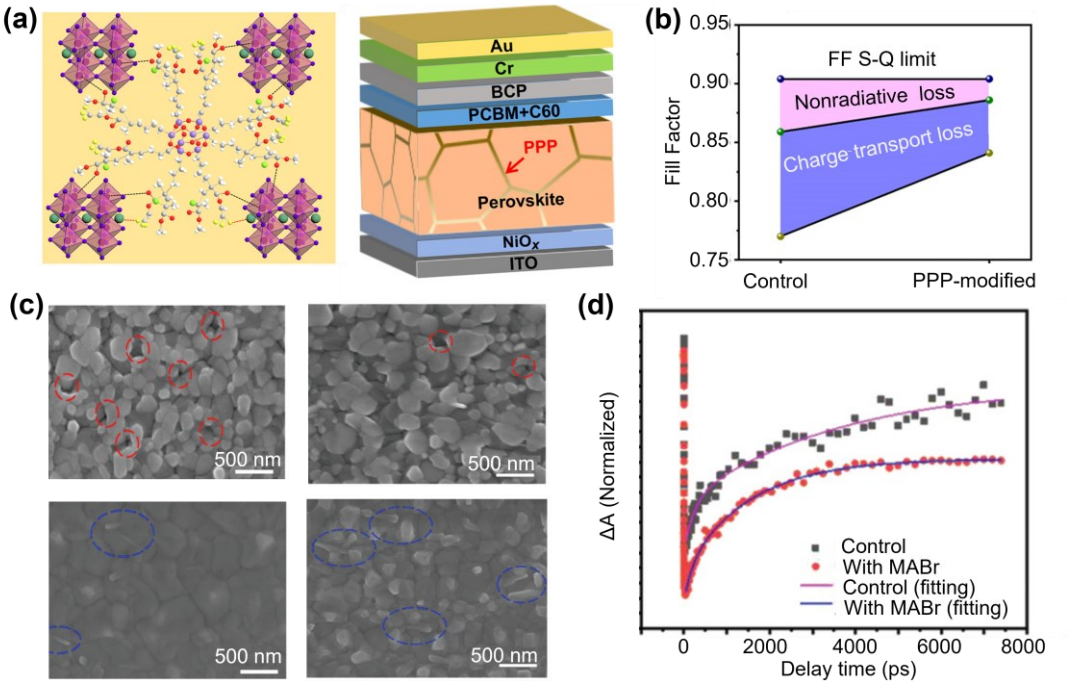

Fig. 8. (a) The interaction between PPP polymer and perovskite and device structure of IPSCs. (b) The calculated FF loss. Reproduced from Ref. [113] with permission from the American Association for the Advancement of Science. (c) SEM images of

different perovskite thin film with various concentration of MABr. (d) TA spectra of perovskite films. Reproduced from Ref. [126] with permission from John Wiley and Sons.

3.2.3 Surface treatment via Inorganic bonding

The weak bonding nature of organic materials with perovskite is undesirable and may lead to stability issues in some cases. Beyond organic materials, using inorganic materials has been considered an efficient passivation strategy for IPSCs. The sulfur-containing compounds are developed as novel passivators because of the strong coordination nature of Pb–S bond. Water-insoluble lead oxysalt was introduced as a capping layer by Huang and co-workers [19]. The oxyacid ions are expected to react with perovskite to form wide-bandgap $PbSO_4$. The sulfate anions play a dominant role in ion compensation and surface passivation effect, which ultimately improve device performance and stability. As shown in Fig. 9(a), the compact and uniform lead sulfate layer is formed between perovskite and C_{60} films. Moreover, the ion migration is effectively suppressed, which may be originated from the immobilization of surface defects by the lead sulfate layer. The water resistance property of lead sulfate on perovskite single crystal is also presented. After coating with a lead sulfate layer, the device can remain black for 3 min, whereas the control film is quickly decomposed into PbI_2. Similarly, lead-sulfur (PbS) is deposited on the top surface of perovskite to construct heterojunctions for IPSCs via surface sulfidation treatment (SST) (Fig. 9b)[34]. A shallow Fermi level with more n-type properties can be obtained by SST, implying that an extra back-surface field shows the same direction with the built-in potential. The strong coordinative nature of Pb-S bonds can suppress interfacial recombination and inhibit degradation reactions in the device. Moreover, the lattice matching of PbS and perovskite can stabilize the FA-based perovskite structure. Consequently, the SST-IPSCs achieve an ultra-high efficiency of 24.3% and respectively retain 91.8% and 90% of their initial efficiencies after aging at 85 °C for

2200 h and MPP tracking for 1000 h. Metal halide materials are also reported as efficient post-treatment candidates for perovskite solar cells. A trace of indium bromide ($InBr_3$) is adopted as a beneficial surface n-doping of perovskite, which is able to construct n/n^+ homojunction at the top of perovskite's surface [112]. It is demonstrated that the work function of the doped perovskite film is downshifted by 0.49 eV compared to control film. This leads to the band bending at the interface of perovskite/ETL and regulates the interfacial charge dynamics with minimized electron injection barrier. As a result, the IPSCs with $InBr_3$ surface treatment attain a high PCE of 22.2% and V_{oc} of 1.18 V, respectively.

Most recently, an organometallic compound, ferrocenyl-bis-thiophene-2-carboxylate ($FcTc_2$), was developed as an efficient interface functionalization agent for IPCs by Zhu and co-workers [35]. It was demonstrated that $FcTc_2$ could provide strong chemical Pb-O bonding with perovskite and enhance electron extraction and transfer through electron-rich and electron-delocalizable ferrocene units. In this study, peak force infrared (PFIR) spectroscopy was conducted to confirm the signal of MA ions in perovskite; this signal variation of MA can represent the stability of perovskite films. As shown by PFIR mapping in Fig. 9(c), the intensity and distribution of MA^+ cations were well maintained in the $FcTc_2$-treated sample after 1000 h of aging, where the MA signal in the control sample was significantly reduced in intensity and distribution was broadened. This result indicated that $FcTc_2$ was able to block the movement of surface ions, leading to a more uniform and stable distribution of surface components along with highly thermal-stable and water-resistant perovskite film. The device delivered an efficiency up to 25% (certificated 24.3%) with ultra-high stability. Also, the devices showed excellent long-term stability (at room temperature with AM 1.5 G simulated solar illumination, T_{98} > 1500 h), damp-heat stability with IEC61215:2016 qualification (85 °C and 85% RH, T_{95} > 1000 h) and cycle stability (cycle shocks of −40 °C and 85 °C, T_{85} > cycles).

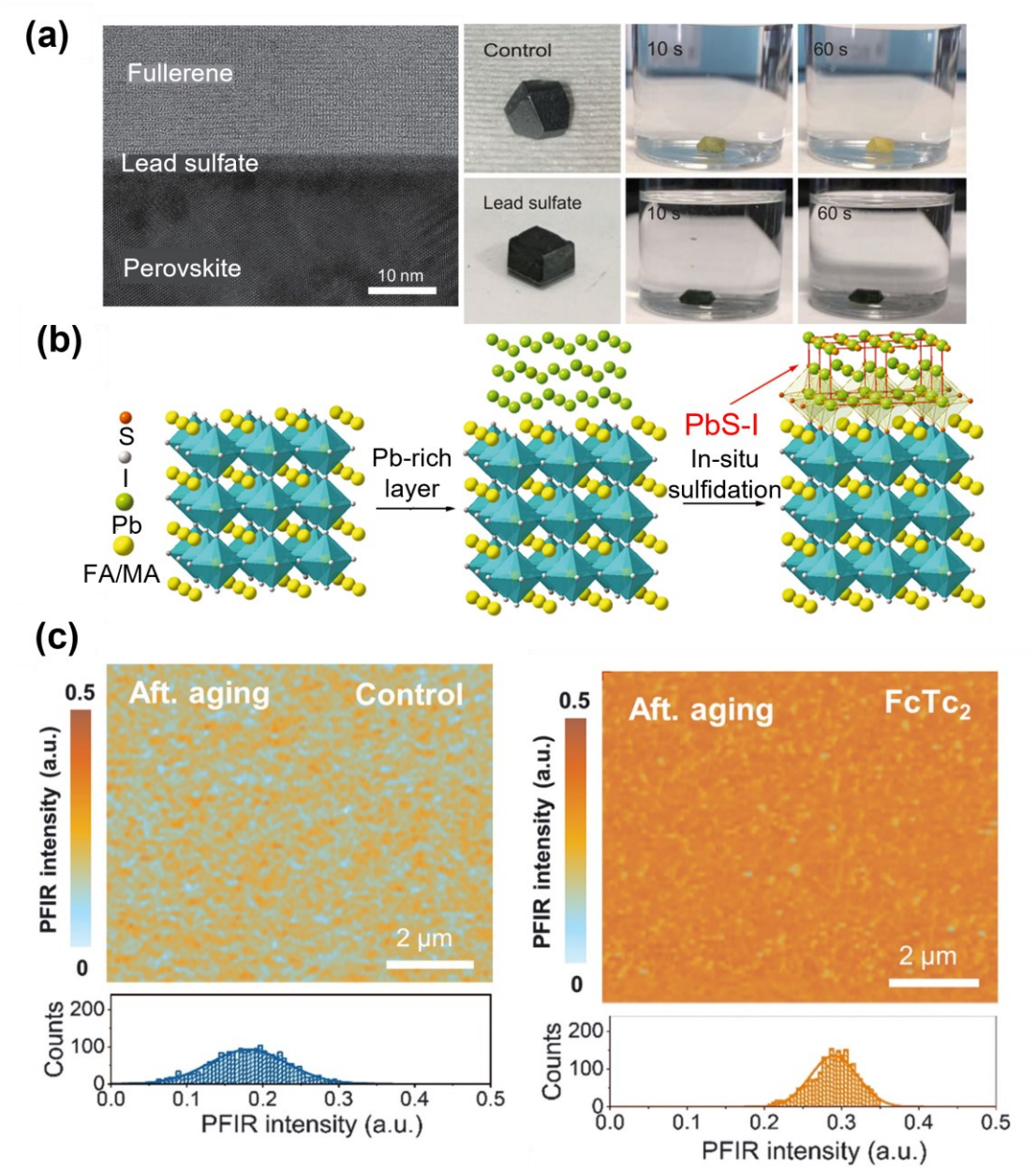

Fig. 9. (a) Cross-sectional HR-TEM image of perovskite interface and enhanced water resistance and suppressed ion migration by the lead sulfate surface. Reproduced from Ref. [19] with permission from the American Association for the Advancement of Science. (b) Schematic diagram of surface sulfidation treatment (SST). Reproduced from Ref. [34] with permission from the American Association for the Advancement of Science. (c) Peak force infrared mapping of MA in the control and $FcTc_2$-treated perovskite films after aging. Reproduced from Ref. [35] with permission from the American Association for the Advancement of Science.

3.3 Summary and perspectives of interfacial layer

The large efficiency loss in IPSCs is due to severe interfacial recombination caused by imperfect interfaces. Developing interfacial layer is essential for further improvement of IPSCs. The efficiency gap between IPSCs and regular structure PSCs will be decreased and eventually even out. But several issues should be addressed, first, the weakness of bottom interface should be solved due to the downward growth direction. It is important to look into novel HTLs, including those made of organic and inorganic materials. Additionally, a thorough evaluation of the buried interface is recommended to minimize interface defects and residual strain. In addition, high-density traps on the exposed top surface are also a major contributor to surface recombination. Effective surface passivation strategies should be carried out to migrate the energy loss for high-efficiency and ultra-stable IPSCs.

4. Single-junction IPSCs with high efficiency

In addition to the interface engineering for both bottom interface and top interface, manipulating perovskite films by additives engineering and novel coating strategies is denoted as efficient approaches to achieve high-efficient IPSCs. The recent advances on the development of additives and strategies towards high-efficient single-junction IPSCs are discussed in this section [132,133].

4.1 Additives for IPSCs

Additive engineering is widely used and plays a vital role in developing high-efficient IPSCs. Due to the interaction nature of the additives with perovskite compounds such as lead cation and halides by chemical bonding or hydrogen bonding. Various additives, such as ion liquids, small molecules and organic spacers, can be applied for IPSCs [26,134–147].

Snaith and colleagues utilized 1-butyl-3-methylimidazolium tetrafluoroborate ($BMIMBF_4$) ion liquid into perovskite precursor, as shown in Fig. 10(a) [134]. The $BMIMBF_4$-based IPSCs showed improved photovoltaic performance and enhanced V_{oc}

and FF with negligible hysteresis. They also demonstrated that the $BMIM^+$ cation existed throughout the perovskite film and reacted with PbI_2, whereas BF_4^- anion mainly accumulated at the buried interface of perovskite and compensate for the halide vacancy. More importantly, the $BMIMBF_4$-based IPSCs showed extraordinary stability, including air stability, operational stability, and retaining 80% of initial value under 1072 h continuous heating at 75 ℃ (Fig. 10d).

In addition to ion liquids, organic materials with functional groups are developed to interact with perovskite and improve the device performance of IPSCs. Interestingly, a complete transformation of p-type to n-type on the perovskite surface of $MAPbI_3$ IPSCs was reported for the first time (Fig. 10b) [138]. By doping 0.1 wt% of capsaicin into $MAPbI_3$ precursor, this transformation was demonstrated by 470 meV decrease in W_F as well as the shifted VBM (Fig. 10c); these findings can be verified by Hall Effect measurement. Meanwhile, the electron transport and defect passivation were simultaneously attained by the p-n homojunction perovskite, resulting in one of the highest efficiencies among $MAPbI_3$-based IPSCs.

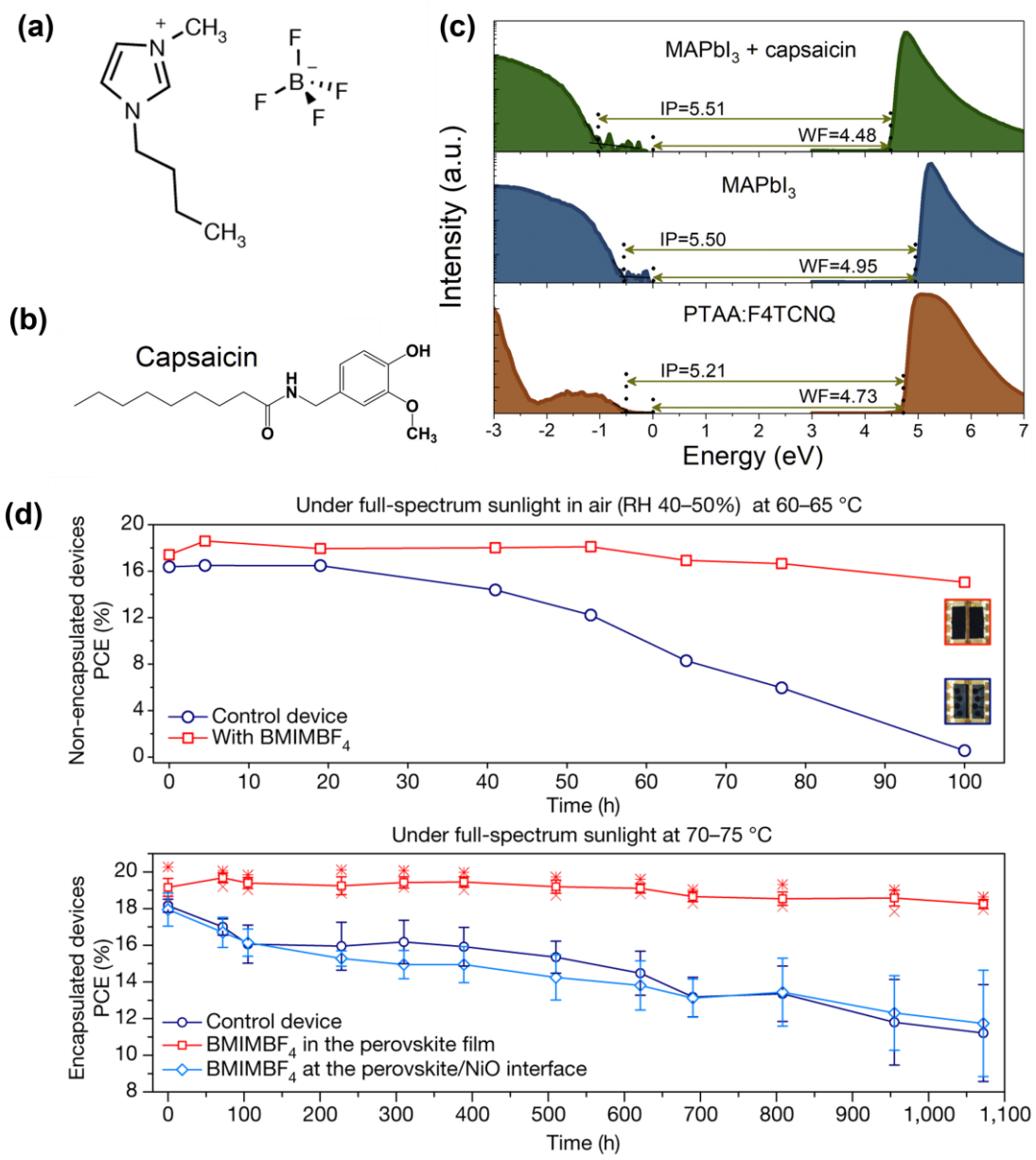

Fig. 10. (a) Molecular structure of $BMIMBF_4$. Reproduced from Ref. [134] with permission from the Nature Publishing Group. (b) Molecular structure of capsaicin. (c) UPS and energy level of perovskite films. Reproduced from Ref. [138] with permission from Elsevier. (d) Device stability of $BMIMBF_4$-based devices. Reproduced from Ref. [134] with permission from the Nature Publishing Group.

Except for small molecules, organic spacers are prominent candidates for IPSCs as additives. A trace of surface-anchoring alkylamine ligands (AALs) with different chain lengths is developed by Bakr and co-workers as additives into perovskite

precursor [26]. It is suggested that the introduction of a small amount (<0.3 mol%) of AALs does not form 2D/3D perovskite heterojunctions (require >5 mol% AALs) but significantly change the optoelectronic properties of perovskite films. The energy diagrams show that the VBM and CBM of AAL-modified films are almost the same as the pristine films. Nevertheless, the W_F shifts to the vacuum level by about 170 meV and the E_F shifts to CBM by 200 meV, indicating that the AAL-modified films become more n-type, which may be ascribed to the modification of surface termination by AALs. Meanwhile, the assembly of long-chain AALs on perovskite grains limits the tilting of the grains during the growth, resulting in a (100)-oriented film with a lower defect density compared to randomly oriented films (Fig. 11a). Thus, the long chain AAL OAm-based IPSCs delivered improved efficiencies and achieved a PCE of 23%. Another way to improve both efficiency and stability of IPSCs is constructing low dimension (LD) perovskite along with 3D perovskite to in-situ form 2D/3D perovskite heterojunction. However, few reports that used pre-crystallized LD perovskites as additives for IPSCs, because most commonly used LD perovskites are susceptible to reconstructing to n values in the 3D precursor, which influences the perovskite crystallization [148,149]. Yao and colleagues employed 2D propargylammonium chloride perovskite ($(PYA)_2PbCl_4$) into 3D perovskite precursor [140]. Fig. 11(b) illustrates the classic strategy and pre-crystallization strategy. For the thin films prepared by the pre-crystallization method, the seeds of the target 2D perovskite stay in chemical equilibrium with the 3D precursor and solvent. The 2D $(PYA)_2PbCl_4$ is shaped as pure phase 2D perovskite (n=1) embedded in the 3D perovskite grain boundaries, which can not only passivate the defects but also improve the charge collection. Thus, the IPSCs with 2D/3D junctions show significantly improved efficiency and stability.

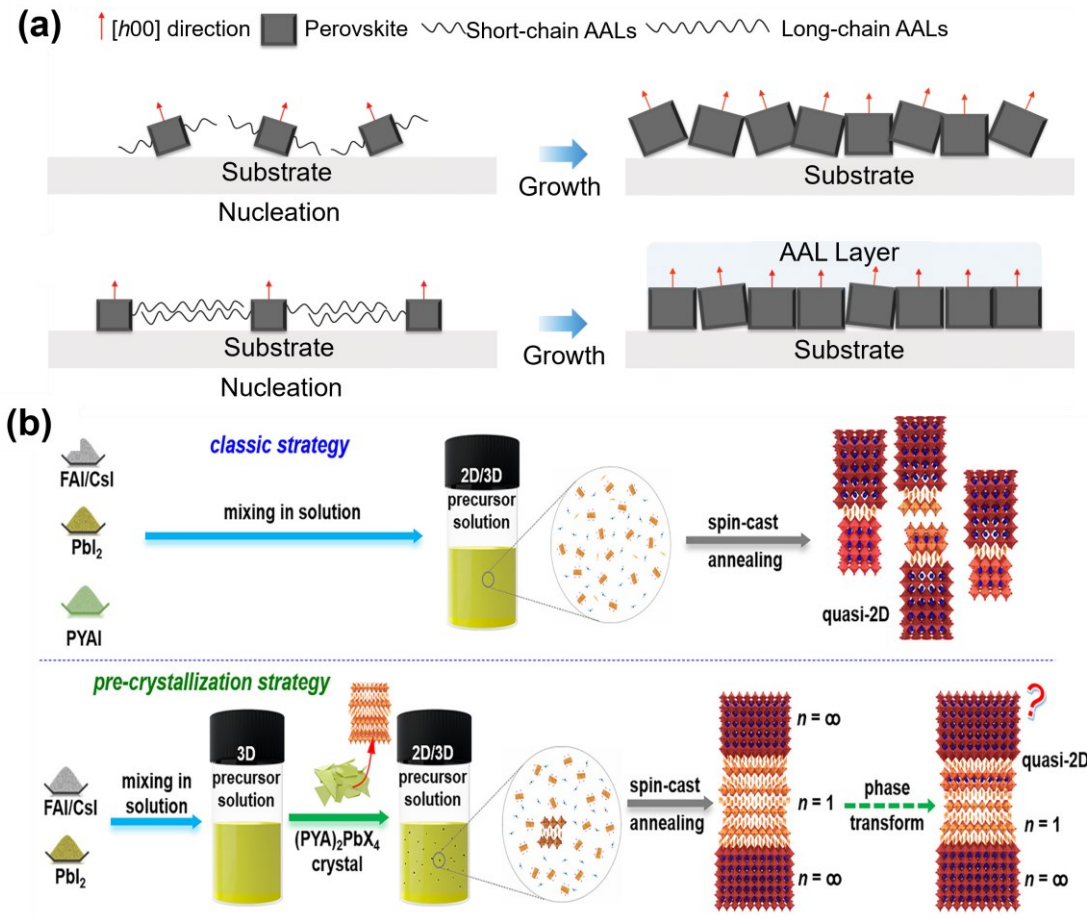

Fig. 11. (a) Illustration of the influence of the length of AALs chain on the crystallization of perovskite films. Reproduced from Ref. [26] with permission from the Nature Publishing Group. (b) Schematic of two synthetic strategies for the 2D/3D bulk heterostructure films. Reproduced from Ref. [140] with permission from the American Chemical Society.

4.2 Emerging coating methods for IPSCs

Though most of the reported high-efficiency PSCs are based on traditional spin-coating methods, the coating method is highly susceptible to environmental conditions, such as controlled humidity and oxygen [150]. Recently, universal coating methods were developed for high-efficient IPSCs and their up-scale applications [151].

Blade-coating is denoted as an efficient strategy towards high efficiency and stability for printable solar cells [30,152–155]. Generally, both regular and IPSCs can be fabricated by the coating technologies, including blade coating, spray coating, and

spray printing etc. Considering the scope of application and commercialization, IPSCs with better stability exhibit greater promise. The emerging coating technologies are effective for fabricating large-scale cells and modules, which is essential for commercialization of perovskite photovoltaics. Besides, the fabrication processes of IPSCs are easier than that of regular devices as the HTL can be PTAA polymer which is easier to coat than small molecule. Currently, Huang et al. has reported an all-blade-coating strategy for the fabrication of efficient IPSCs, which pushes the commercialization of perovskite photovoltaics one step closer [156]. Li and colleagues report that zwitterionic surfactant, tetradecyldimethyl(3-sulfopropyl)ammonium hydroxide inner salt (TAH) can be developed as appropriate additives for room-temperature blade coating IPSCs [135]. As shown in Fig. 12(a), the TAH molecule presents hydrophobic and hydrophilic terminal groups with both positive and negative functionalized groups. The accelerated nucleation process of TAH-based perovskite at the intermediate phase verified by in situ GIWAXS is beneficial to obtain dense perovskite films with low defect density. The TAH is self-assembled at the perovskite top surface, forming a moisture barrier spontaneously. As a result, the TAH-based devices show enhanced PCEs up to 22% for both inverted and regular structures. More recently, Huang et al. reported partially-replaced common DMSO with lead-coordinating additive carbohydrazide (CBH) in blade-coating IPSCs [29]. Similar to DMSO, the CBH has a coordination ability by means of C=O bond but can retard the fast crystallization speed of perovskite (Fig. 12b). Compared to the DMSO-based perovskite film with abound voids at the bottom interface, the CBH-based film presented a dramatically lower quantity of voids, owing to the nonvolatility of CBH. In addition, the degradation process could be suppressed because degradation caused by charge accumulation and recombination is exemplified. As a result, CBH-based devices delivered a high efficiency of 23.8% at small scales. When the size is scaled up to 17.9 and 50.1 cm^2, the efficiencies of minimodules approach 20.1% and 19.7%, respectively (Fig. 12c).

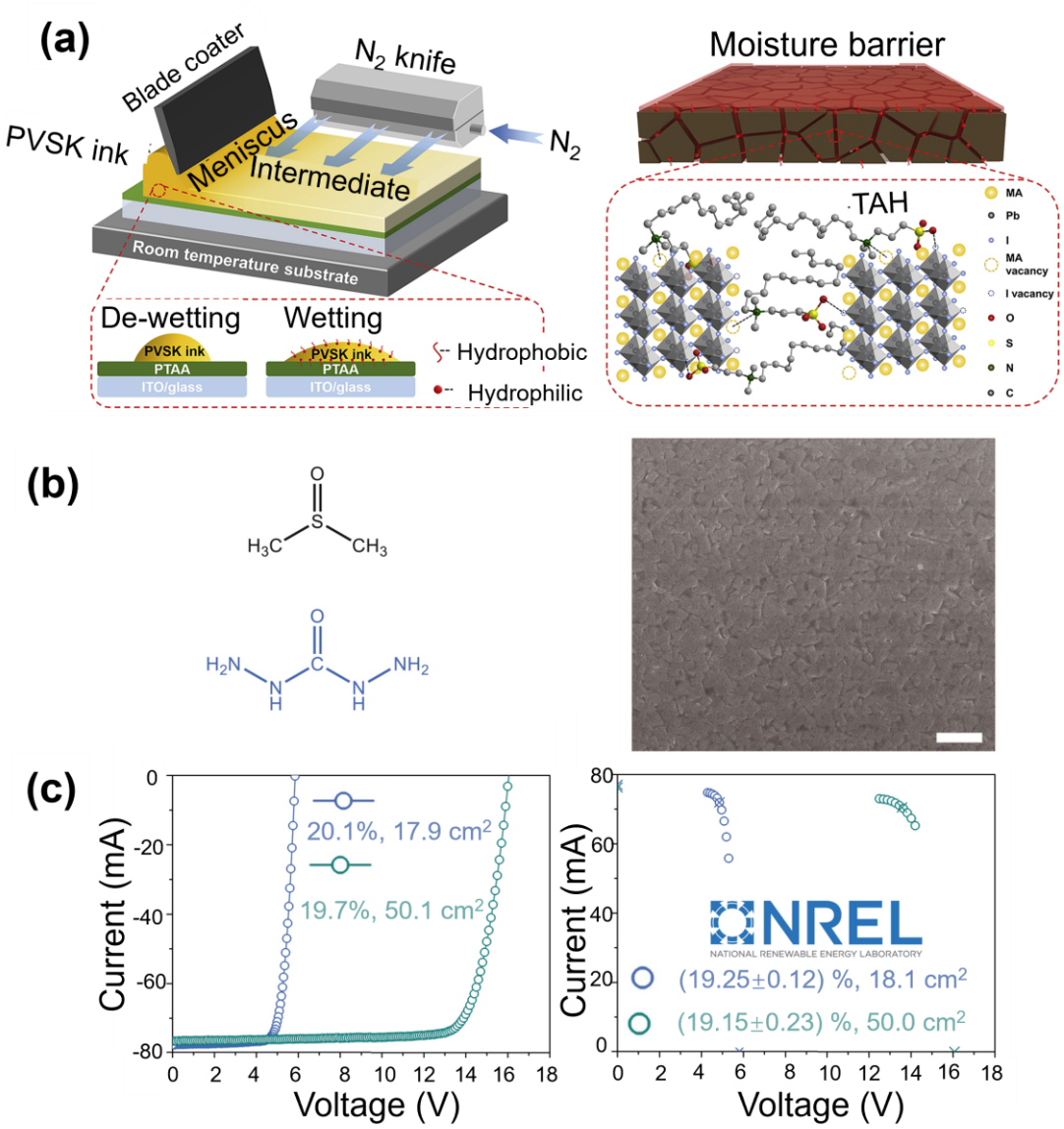

Fig. 12. (a) Schematic illustration of the zwitterionic surfactant-assisted meniscus coating at room temperature. Reproduced from Ref. [135] with permission from Elsevier. (b) Molecular structure of CBH and SEM image of the perovskite-substrate interfaces. (c) Photovoltaic performance of perovskite minimodules. Reproduced from Ref. [29] with permission from the American Association for the Advancement of Science.

IPSCs can be constructed at a low temperature that is suitable for flexible applications, in contrast to regular PSCs that need higher temperature annealing for ETLs. However, to obtain the α-phase FA-perovskite phase and high-quality perovskite

films, the annealing temperature requirement for perovskite always exceeds 120 ℃ that is not highly desirable for flexible substrates. Herein, developing low-temperature processed perovskite film with high crystallinity perovskite is required for low cost flexible IPSCs. Room-temperature (RT) perovskite ink has been reported by Priya and colleagues [23]. This RT method takes advantage of solubility of the perovskite intermediate phase in alcohol with amine molecules, which allows fast solvent evaporation and quick phase transition into tetragonal β-phase perovskite films RT. As illustrated in Fig. 13(a), after writing a text on paper at room temperature using this fast-crystallizing perovskite ink, the perovskite ink tends to crystallize after several seconds. This ink is compatible with spin-coating and blade-coating methods. Meanwhile, SEM images exhibit a high-quality film morphology consisting of compact and dense hexagonal grains with an average size of around 700 nm. As a result, the RT perovskite crystals show ultrahigh preferred orientation with a charge diffusion length close to 3 μm and PCEs of 23.1% for IPSCs.

Pure α-$FAPbI_3$ perovskite with a suitable bandgap of ~1.45 eV has attracted much attention for high-efficient IPSCs. However, the formation of α-$FAPbI_3$ perovskite phase usually requires high temperature for thermal annealing (>150 ℃) to complete the phase transformation from non-perovskite δ-$FAPbI_3$ phase to α-$FAPbI_3$ perovskite phase [157,158]. Cheerfully, additive-free and low-temperature processed α-$FAPbI_3$ IPSCs have been reported by Briscoe and colleagues [159]. Compared to traditional thermal annealing (TA) $FAPbI_3$ perovskite, the aerosol-assisted crystallization (AAC) method carries excellent advantages for inhibited phase segregation, enhanced grain orientation and improved stability. The purpose of using AAC is to generate a stable laminar flow over the film. This leads to the controlled evaporation of solvent droplets in the aerosol near the film's surface, creating a continuous "source" of solvent vapor that enters the film uniformly. For the AAC method, the as-formed perovskite films are firstly annealed at 100 ℃ for a few minutes followed by exposure to aerosol atmosphere (DMF/DMSO) and further dried at 100 ℃. TA films contain irregular grains, while

AAC films show larger grains in the lateral direction; the average lateral grain size increases from 310 nm (TA) to 890 (AAC 1 min), 1060 nm (2.5 min) and 1170 nm (5 min). Moreover, the stability of the as-prepared perovskite film is examined under 1 sun illumination in ambient air with 75% ± 5% relative humidity. As performed in Fig. 13(b), TA films are decomposed much faster than AAC films. Moreover, the residual strain can be released in AAC perovskite films, as illustrated in Fig. 13(c). The perovskite presents a higher expansion coefficient than ITO; the contraction is mainly allowed in the out-of-plane direction, leaving an in-plane tensile and out-of-plane compressive strain. In the AAC route, the lower annealing temperature (100 °C) results in less lattice expansion at the beginning, with the released residual tensile strain upon the growth of solvent-induced crystals. And the vapor entry is maximized at the grain boundaries, allowing a thorough microstructural reconstruction at the edges of existing $FAPbI_3$ grains with a more thermodynamically balanced configuration.

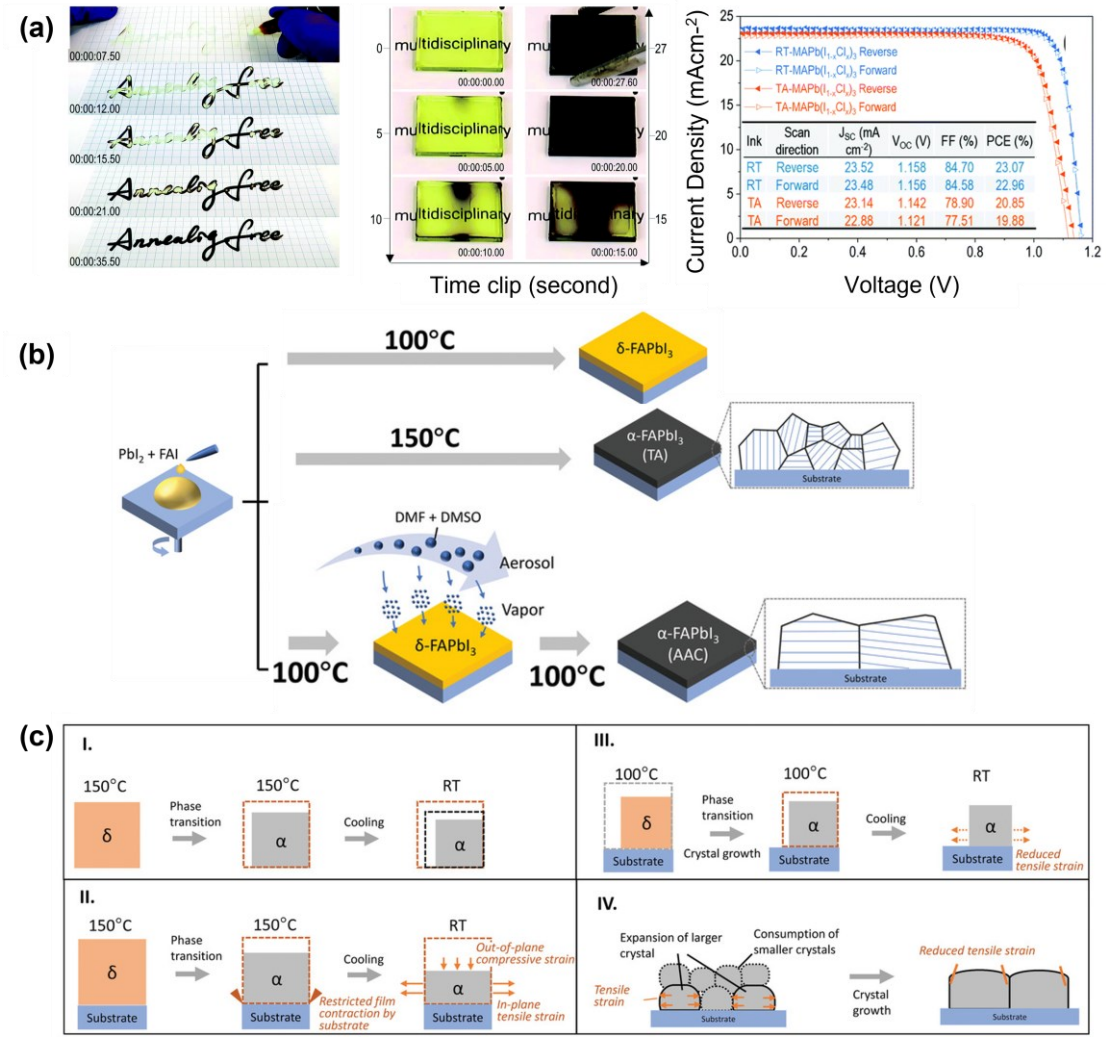

Fig. 13. (a) Images of annealing-free perovskite ink and device performance of annealing-free IPSCs. Reproduced from Ref. [23] with permission from the Royal Society of Chemistry. (b) Scheme of TA method and AAC method. (c) The schemes of released residual strain in AAC perovskite films. Reproduced from Ref. [159] with permission from John Wiley and Sons.

4.3 Summary and perspectives of high-efficiency single-junction IPSCs

Since the benefits of IPSCs have been recognized, significant advancement in the PCEs of single-junction IPSCs has been made, allowing them to catch up to their n-i-p counterparts. Despite the inspiring research that summarized, there are still certain obstacles and perspectives that need to be addressed to advance the research for the future development of single-junction IPSCs. Firstly, to reduce the bulk trap density,

additives with functional groups can be applied to improve the crystallinity and reduce trap states for IPSCs.

In addition, fullerene and its derivates are commonly used in IPSCs, however, the major concern is that poor hole blocking and weak passivation properties of fullerenes are remained to be solved. Interestingly, the use of solution-processed inorganic electron transport layers with high conductivity, such as SnO_2 and TiO_2, is expected to provide IPSCs with improved stability and cost benefits.

Additionally, further study is required for IPSCs with pure α-$FAPbI_3$ (Eg~1.48 eV) and ideal bandgap (Eg~1.33 eV) bases that have the potential to attain high efficiency. Moreover, except for the development of multiple-layer solar cells, simplified-structured PSCs with the structure of ITO/Perovskite/Metal with eliminated HTL and ETL are regarded as promising strategy for both low cost and high efficiency.

5. Tandem and integrated solar cells

Currently, the highest record PCE of single-junction PSCs was reported as 25.7%, close to the Shockley-Queisser (SQ) limit [1]. To further improve the efficiency beyond the S-Q limit, tandems or integrated solar cells can be constructed that effectively cover more absorption regions of the solar spectrum. PSCs with inverted configurations are quite suitable for fabricating tandems due to the facile fabrication process and reduced parasitic absorption [18]. In this part, wide-bandgap and narrow-bandgap PSCs-based inverted structures are discussed in terms of their challenges, strategies, and recent progress.

5.1 Wide-bandgap IPSCs

PSCs with wide bandgaps (~1.7 eV) are generally applied in the perovskite tandem solar cells as the front sub-cells, which are responsible for absorbing the high-energy photons [160,161]. Wide-bandgap perovskites used in tandem cells typically contain mixed iodine (I) and bromine (Br) anions. The bandgap of perovskites can be tuned by changing the I/Br ratio. The higher content of Br improves the bandgap of perovskites. Ideally, the voltage loss is similar in all compositions of perovskites, however, it increases when the bandgap increases [162,163]. The voltage loss of Br-rich perovskite is much more significant than that of low-Br content perovskites. The large V_{oc} deficit of wide-bandgap PSCs is mainly ascribed to the photoinduced phase segregation and lower carrier lifetime in Br-rich wide-bandgap perovskite. The voltage loss of some typical inverted wide-bandgap PSCs is summarized in Fig. 14(a) [93,134,160–162,164–179].

To tackle the above issues, researchers have devised various strategies, such as compositional and additive engineering to stabilize the perovskite phase and reduce trap-state density, as well as interface engineering to improve the interfacial quality and match energy levels. For example, Wolf et al. developed perovskites with various bandgaps by altering the I/Br ratio, discovering that the low-Br content reduces the stability issue caused by halide segregation [170]. Besides, McGehee et al. proposed a

compositional tuning strategy by using more Cs content at the A-site rather than more Br at the X-site to stabilize the 1.75 eV-bandgap perovskite (Fig. 14b). Moreover, a high V_{oc} (1.17 eV) and improved PCE (16.3%) can be obtained (Fig. 14c) [166]. According to these reports, the bandgap and photostability of perovskites can be well balanced by fine compositional tuning.

Additive engineering is another intriguing strategy to suppress photoinduced phase segregation and prolong the carrier lifetime by improving perovskite-film quality and reducing halide ion migration. For example, Sun et al. reported that the incorporation of K ions can enhance the performance of wide bandgap IPSCs [180,181]. The improvement is attributed to the synergistic effect of lattice occupation and grain boundary passivation, in which K ions can partially interact with PbI_2 to form 2D K_2PbI_4 phase at grain boundaries, efficiently suppressing phase segregation and significantly improving the PCE (from 15.28% to 17.94%). Moreover, Shin et al. reported an anion-engineering strategy by incorporating mixed I and SCN anions into the perovskite precursor, which enhanced the carrier lifetime and reduced defect density [171]. As a result, the 1.7 eV-bandgap PSC showed a high PCE of 20.7% and improved photostability, retaining more than 80% of its initial PCE after 1000 h of continuous illumination. Besides, Wolf et al. introduced carbazole additive into the perovskite precursor to stabilize halide species, passivate the deep-level defects, and suppress the phase segregation in wide-bandgap perovskites (Fig. 14d) [164]. In outdoor tests, the carbazole-based perovskite tandem maintained more than 93% of its initial efficiency for over 40 days, indicating that the phase stability of the wide-bandgap perovskite is greatly improved. In a recent report, Snaith et al. used an ionic liquid additive (1-butyl-1-methylpipiderinium tetrafluoroborate) to simultaneously reduce the nonradiative carrier recombination at HTL/perovskite and perovskite/ETL interfaces by mitigating the surface recombination velocity [179]. Upon the incorporation of an ionic additive and a thin LiF interlayer, the MA-free wide-bandgap IPSCs exhibited a high PCE of ~17% with an improved V_{oc} of 1.22 V. Other additives, such as amine salts, imidazolium

and piperidinium have also been introduced into the perovskite precursors to tackle the photo-instability issues [134,167,176].

Another challenge that plaguing the development of wide-bandgap IPSCs is the poor interfacial quality, especially the HTL/perovskite interface. In wide-bandgap IPSCs, the undesirable HTL/perovskite contact leads to more severe effects, such as voids accelerate the migration of halide ions. Introducing passivation layer and developing alternative HTLs are efficient methods to address the interface issues. For example, Fang et al. constructed 2D/3D perovskite heterojunction interface using 2-thiopheneethylammonium chloride (TEACl). The formation of 2D perovskite passivated the defects located at the upper part and grain boundary of perovskite films. As a result, the TEACl-treated wide-bandgap IPSCs demonstrated improved PCEs and stability [115,182]. Moreover, Tan et al. replaced PTAA with more hydrophilic NiO to fabricate the 1.77-eV-bandgap IPSCs,[165]. Hou et al. used benzylphosphonic acid to passivate the NiO HTL to suppress the interface recombination of NiO/perovskite and boost the V_{oc} up to 1.26 V in a 1.79 eV-bandgap PSCs [175]. Besides, Albrecht et al. developed a self-assembled and methyl-substituted carbazole monolayer as the HTL facilitated the hole extraction and reduced nonradiative recombination at the hole-selective interface [93]. Perovskites deposited on ITO/Me-4PACz substrate, which was more stable over time according to the time-dependent photoluminescence spectra (Fig. 14e). Based on this HTL, the 1.68-eV-bandgap PSC exhibited a high PCE of 20.8% and an improved V_{oc} of 1.234 V. Besides, the monolithic tandem constructed by integrating this wide-bandgap PSC with a silicon heterojunction solar cell showed the highest certified PCE of 29.15%.

To date, composition engineering has become more and more mature, and the composition of efficient wide-bandgap PSCs has also tended to be suitable. Most high-performance wide-bandgap IPSCs employ tri- or di-cations combined with mixed halide anion as perovskites absorbers, demonstrating a bandgap region of 1.65–1.8 eV. By contrast, additive and interfacial engineering still play essential roles in stabilizing

the perovskite phase and improving photovoltaic performance. With these practical strategies further optimize wide-bandgap IPSCs, the PCE of monolithic perovskite/silicon tandems exceed 30% with a large-scale in the near future, and the stability is predicted to meet the requirements of commercialization.

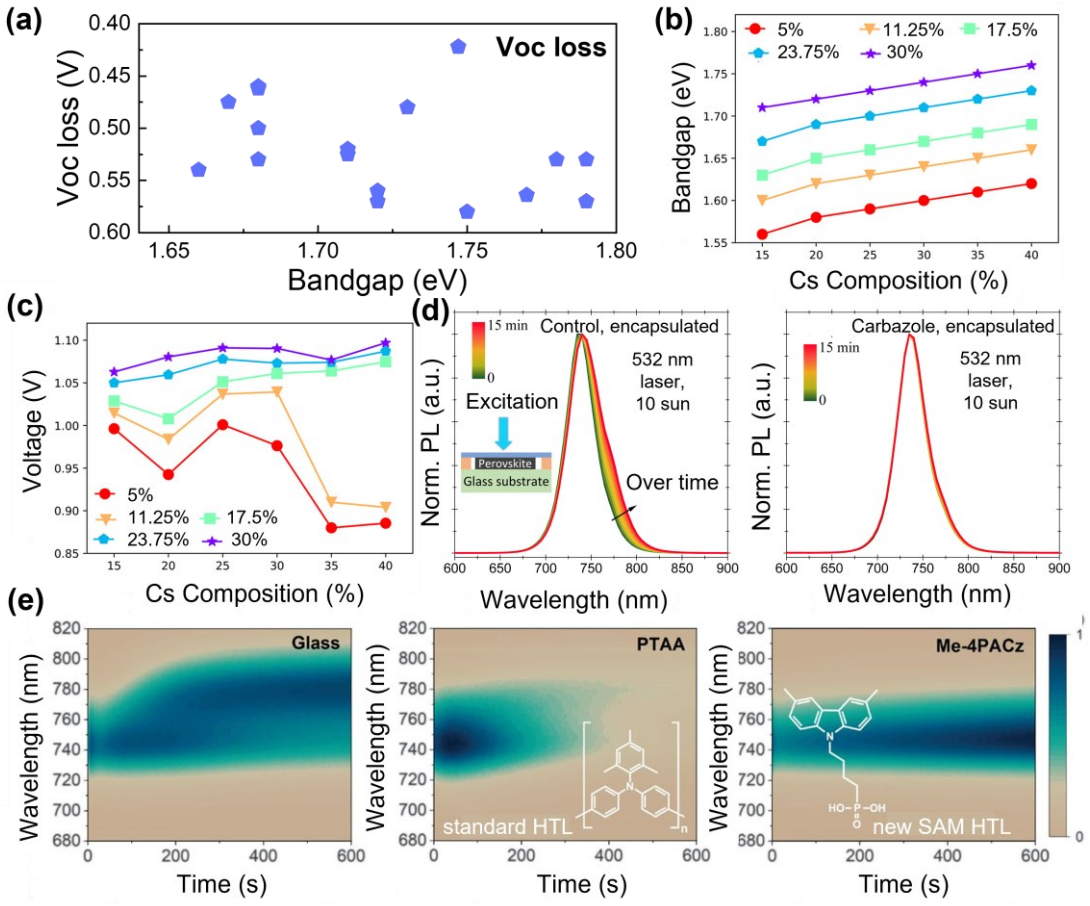

Fig. 14. (a) The voltage loss of some typical inverted wide-bandgap PSCs. (b) Bandgaps versus various $Cs_xFA_{1-x}Pb(Br_yI_{1-y})_3$ compositions. (c) V_{oc} versus various $Cs_xFA_{1-x}Pb(Br_yI_{1-y})_3$ compositions. Reproduced from Ref. [166] with permission from the American Chemical Society. (d) Time-dependent PL spectra for the control and carbazole-treated encapsulated perovskite films [164] with permission from Elsevier. (e) Time-dependent PL spectra of perovskite films deposited on glass, PTAA, and Me-4PACz. Reproduced from Ref. [93] with permission from the American Association for the Advancement of Science.

5.2 Narrow-bandgap Sn-Pb IPSCs

Broadening the absorption spectrum is an effective way to improve the efficiency of solar cells. The construction of Sn-Pb perovskite can expand the absorption window to the near-infrared region (>900 nm) [183,184]. This ideal bandgap allows Sn-Pb PSCs to improve the solar energy utilization of single-junction PSCs and construct all-perovskite tandems [185]. However, the construction of high-performance Sn-Pb PSCs is facing two main challenges. First, it is difficult to obtain complete coverage and high-quality Sn-Pb perovskite films, mainly due to the fast perovskite crystallization process. Second, Sn^{2+} is easily oxidized to Sn^{4+} in Sn-Pb halide perovskites under air atmosphere, resulting in high trap-state density, short carrier lifetime, and poor stability [186]. A large number of strategies have been developed to overcome these issues and the recent efficiency development of narrow bandgap IPSCs was summarized in Fig. 15(a) [165,183,185–204].

Additive engineering is one of the most efficient methods to prolong the carrier lifetime of Sn-Pb perovskite. For example, Zhu et al. introduced guanidinium thiocyanate (GuaSCN) into the Sn-Pb perovskite precursor to significantly improve the carrier lifetime of greater than 1 microsecond and diffusion lengths of 2.5 micrometer [188]. Besides, the GuaSCN-modified Sn-Pb perovskite showed high film quality and low defect density. These improved structural and optoelectronic properties enabled 1.25-eV-bandgap Sn-Pb PSC to achieve a high PCE of >20%. In recent work, Xu et al. confirmed that the GuaSCN additive was also favorable in HTL-free Sn-Pb devices [189]. Recently, Tan et al. added 4-trifluoromethyl-phenylammonium (CF_3-PA) into perovskite precursor to passivate defects and increase the carrier diffusion length to >5 micrometer [187]. As a result, the CF_3-PA-modified Sn-Pb PSCs exhibited a high PCE of over 22%. In addition to these conventional additives, antioxidant additives are often used to stabilize Sn^{2+}. For example, Tan et al. adopted a reductive surface-anchoring zwitterionic molecule (formamidine sulfinic acid, FSA) to suppress Sn^{2+} oxidation and passivate trap-states, exhibiting a high efficiency of 21.7% for the single-junction Sn-Pb PSCs and 24.2% for the 1-cm^2-area all-perovskite tandem cell [165]. More

importantly, the encapsulated all-perovskite tandems kept 88% efficiency of its initial value after operating for 500 h under 1-sun illumination at 54–60 ℃ in the ambient atmosphere. In addition, Zhang et al. incorporated a natural antioxidant (caffeic acid, AC) to modulate perovskite crystallization and inhibit the oxidation of Sn^{2+} to Sn^{4+} [197]. The AC-incorporated Sn-Pb IPSCs showed a higher PCE of 19.85% and lower V_{oc} deficit compared to the control. There are many other additives or antioxidant additives used to inhibit Sn^{2+} oxidation, improve film quality, and prolong carrier lifetime, including Sn powder [198], SnF_2 [205], Pb powder [195], BaI_2 [190], CuSCN/glycine hydrochloride complex [192], 4-hydrazinobenzoic acid [194]), and N-(3-aminopropyl)-2-pyrrolidinone [206].

Post-treatment strategy is another effective approach to reduce defects and improve stability. For example, Hayase et al. utilized a Lewis base compound (ethylenediamine, EDA) to transform the p-type surface of Sn-Pb perovskite to n-type by post-treatment; it resulted in a higher built-in potential and lower defect density [201]. The EDA-treated inverted Sn-Pb device exhibited a high PCE of 21.74% and a low V_{oc} loss of 0.39 eV. Besides, Ning et al. constructed a bilayer quasi-2D structure on the perovskite surface by post-treatment using 2-thiopheneethylamine thiocyanate (TEASCN) to reduce defects density and facilitate carrier transfer (Fig. 15b) [199]. As a result, the TEASCN-treated Sn-Pb IPSCs with a high PCE of 21.1% from a credible third-party certification. Moreover, Ye et al. reported a selective targeting anchor strategy to passivate Pb- and Sn-associated traps by spin-coating phenethylammonium iodide (PEAI) and ethylenediamine diiodide (EDAI) on the surface of perovskite [200]. The resultant Sn-Pb device showed a high PCE of 22.51% with an improved V_{oc} of 0.9 eV. Wakamiya and co-workers reported record PCE for narrow-bandgap IPSCs by a dual-interface passivation strategy [207]. On the one hand, ethylene diammonium diiodide ($EDAI_2$) can reduce the trap-state density and facilitate electron extraction on the perovskite surface. On the other hand, glycine hydrochloride (GlyHCl) additive accumulated at the bottom surface can serve as nucleation centers, contributing to the

high crystallinity and large perovskite grain sizes. Upon the design of the dual-interface passivation strategy, the Sn-Pb IPSC with a bandgap of 1.25 eV delivered a record PCE of 23.6% (certificated 23.1%).

Currently, most high-performance Sn-Pb IPSCs adopt PEDOT:PSS as the HTL. However, its acidity and hygroscopic surface are potentially detrimental to the stability of mixed Sn-Pb PSCs. Therefore, modifying the HTL and developing alternative HTLs are quite important to deal with these hurdles. Chen et al. utilized iso-pentylammonium tetrafluoroborate ([PNA]BF_4) ionic salt to modify the surface of PEDOT:PSS to help Pb^{2+} bond on the [PNA]BF_4-modified HTL surface (Fig. 15c) [208]. Upon the modification of PEDOT:PSS with [PNA]BF_4, the champion device showed a high PCE of 20.11% and improved thermal stability at 85 ℃ over 240 h and storage stability over 1200 h. Besides, in a recent report, Hayase et al. developed a combined HTL of 2-(9H-carbazol-9-yl) ethyl] phosphonic acid (2PACz) and phosphonic acid (MPA) to fabricate inverted Sn-Pb PSCs, that demonstrated a champion PCE of 23.3% and an improved V_{oc} of 0.88 V [202].

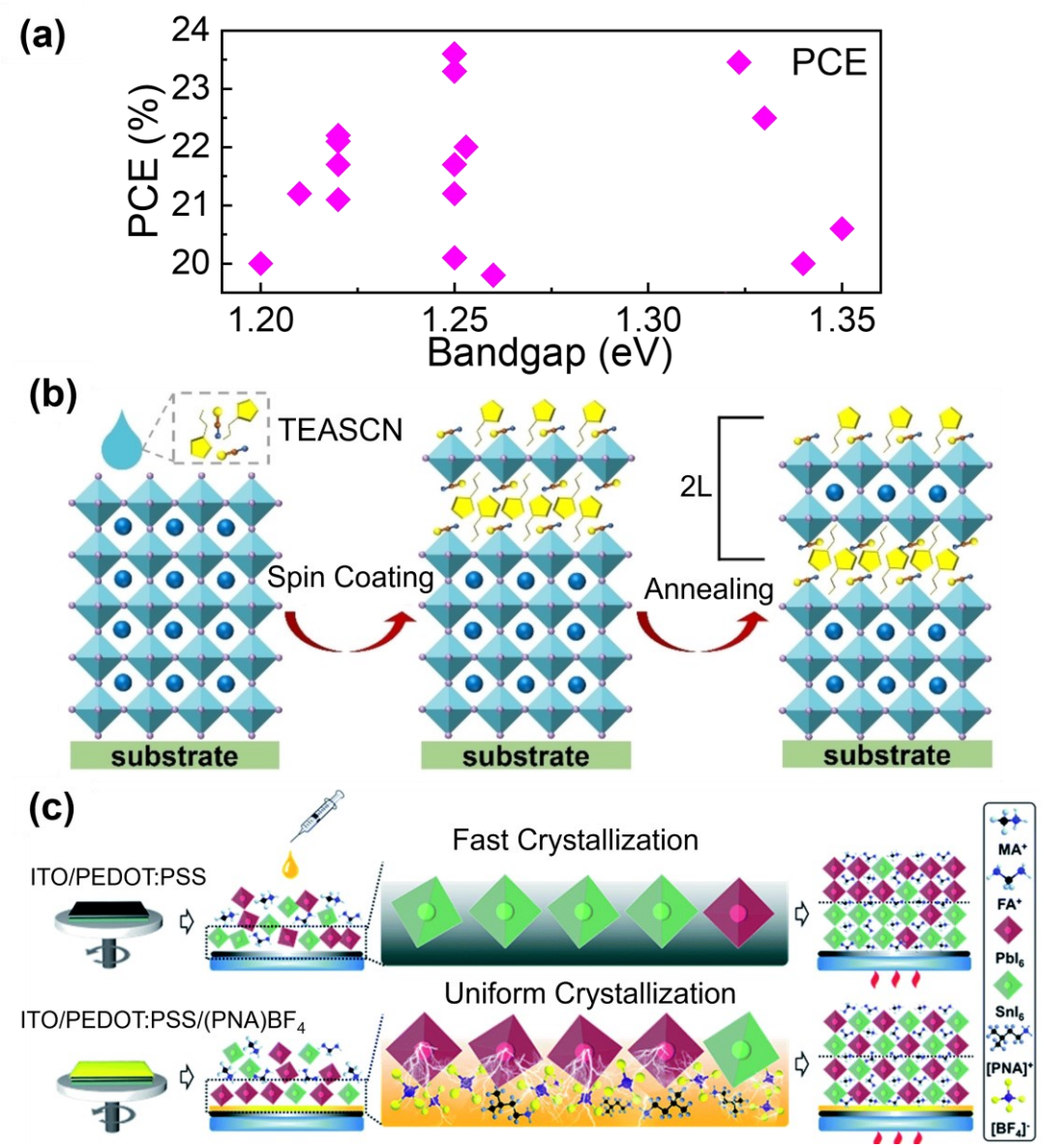

Fig. 15. (a) The recent efficiency development of narrow bandgap IPSCs. (b) Schematic illustration of the structural evolution of perovskite during surface treatment by TEASCN. Reproduced from Ref. [199] with permission from John Wiley and Sons. (c) Schematic illustration of growth of mixed Sn-Pb perovskite on the PEDOT:PSS and [PNA]BF_4-modified PEDOT:PSS. Reproduced from Ref. [208] with permission from the Royal Society of Chemistry.

5.3 IPSCs integrated with bulk heterojunction (BHJ)

The absorption region of the commonly used all-Pb perovskites is below 850 nm, demonstrating large photon loss in the near-infrared (NIR) region. In addition to Sn-Pb or tandem solar cells, integrating ternary-organic BHJ structures into the top layer of

perovskites is also an effective way to extend the photoresponse in the NIR region. He et al. used a p-type polymer (S1), a n-type small molecule (Y6) and PCBM to form ternary BHJ layers on the surface of 1.6-eV-bandgap perovskite film, expanding the absorption to ~980 nm from 775 nm [209]. As a result, the J_{sc} of IPSCs integrated with BHJ improved to 28.06 mA/cm^2, which is among the record values in a single-junction PSC with a 1.6 eV-bandgap absorber. Besides, Russell et al. replaced PCBM with a small-bandgap non-fullerene acceptor (NFA), Y6, and a popular BT-core-based fused-unit dithienothiophen[3,2-b]-pyrrolobenzothiadiazole (TPBT) derivative, resulting in a wider absorption window and improved integrated J_{sc} [210]. Similarly, Jen et al. fabricated an IPSCs integrated with ternary BHJ layers to extend photoresponse over 950 nm [32]. By finely optimizing the BHJ components, this inverted device exhibited an improved PCE of 23.8% and high V_{oc} of 1.146 V. In recent work, Song et al. designed a novel COTIC-4F:$PC_{61}BM$: PTB7-Th ternary organic BHJ to be integrated into the IPSCs, which extends the NIR spectral response to 1100 nm (Fig. 16a) [111]. After simultaneously increasing the NIR and ultraviolet-visible light responses, the PCE of IPSCs integrated with organic BHJ was significantly improved from 20.52% to 23.40%, corresponding to an improved J_{sc} 25.96 mA/cm^2 from 21.79 mA/cm^2. All these reports confirm that the construction of an organic BHJ on the surface of perovskite can greatly improve the J_{sc} as well as the efficiency (Fig. 16b). Most recently, the record efficiency of integrated IPSCs was reported by Xu and co-workers by introducing DTBTI polymer with near-infrared absorption into GABr-modified $FA_{0.6}MA_{0.3}Pb_{0.7}Sn_{0.3}I_3$ perovskite (1.33 eV) [38]. As shown in Fig. 16(c), they proposed that the well-matched energy level alignment and high-quality perovskite film contributed to efficient charge transfer and improved NIR light (Fig. 16d). Resulting in a recorded PCE up to 24.27% among the highest BHJ PSCs, Pb-Sn PSCs and perovskite-organic tandem PSCs [33,175,211].

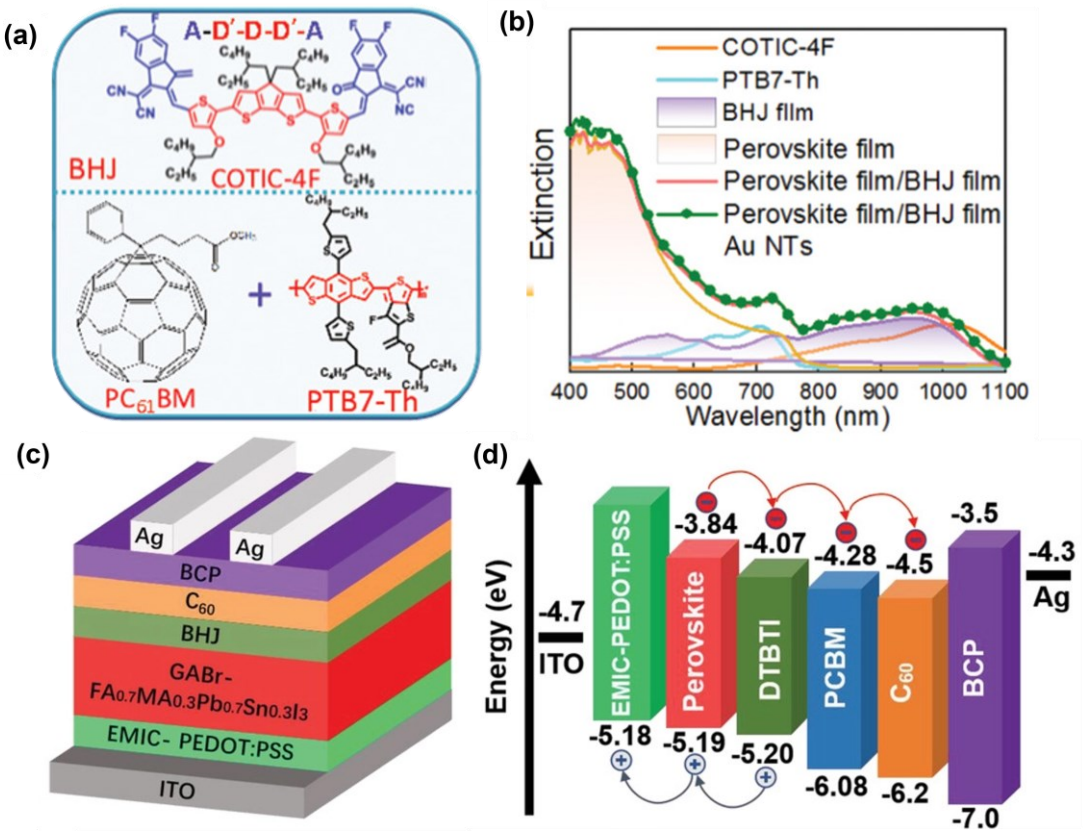

Fig. 16. (a) Molecular structures of the ternary organic BHJ. (b) The extinction spectra of COTIC-4F, PTB7-Th, and various films. Reproduced from Ref. [111] with permission from John Wiley and Sons. (c) The device structure of the integrated IPSCs. (d) The energy of DTBTI and perovskite. Reproduced from Ref. [38] with permission from John Wiley and Sons.

5.4 Summary and perspectives of Tandem and Integrated IPSCs

The inverted structure shows excellent potential for developing tandem and integrated devices to reach high efficiency. The most efficient tandem and integrated PSCs now available are all based on inverted structures, with PCEs for Si/perovskite, perovskite/perovskite, and integrated PSCs exceeding 30%, 26%, and 24% , respectively. However, future progress is hampered by the low efficiency brought on by phase segregation for wide bandgap IPSCs and sensitivity to oxidation for narrow bandgap IPSCs. According to recent study, the following tactics should be taken into consideration for high-efficiency tandem and integrated IPSCs. First, in order to prevent phase segregation for wide bandgap IPSCs, novel HTLs and surface passivation techniques are essential. Additionally, inhibiting the self-oxidation of Sn based narrow bandgap IPSCs can be achieved by precursor engineering and surface engineering to protect Sn from self-oxidation. Moreover, new organic semiconductors with proper absorption and energy level should be investigated to construct efficient integrated IPSCs.

6. Summary

In summary, despite the impressive achievements of IPSCs, there are still a few problems that need to be resolved in order to accelerate future progress. tremendous efforts have been devoted to improving the efficiency of IPSCs. The efficiency of IPSCs has increased over 25% by improving the quality of the perovskite film, alleviating the energy band, passivating defects, and releasing residual strain. In addition, the devices' stability has been greatly improved, which can undertake damp-heat test over 1000 h. Despite the advantages of IPSCs, the suggestions would be useful for research topics with the insight on interfaces, new strategies as well as tandem and integrated IPSCs.

Acknowledgments

G.L. acknowledges the Research Grants Council of Hong Kong (GRF Grant Nos. 15221320, CRF C7018-20G), the Shenzhen Science and Technology Innovation Commission (Project No. JCYJ 20200109105003940, SGDX20201103095403016), the Hong Kong Innovation and Technology Commission (GHP/205/20SZ), the Sir Sze-yuen Chung Endowed Professorship Fund (8-8480) provided by the Hong Kong Polytechnic University, and the Guangdong-Hong Kong-Macao Joint Laboratory for Photonic-Thermal-Electrical Energy Materials and Devices (GDSTC No. 2019B121205001). C. C. thanks the National Natural Science Foundation of China (Grant No. 91963129), the Guangdong Provincial Key Laboratory of Energy Materials for Electric Power (Grant No. 2018B030322001), the Student Innovation Training Program (Grant Nos. 2021S07) from Southern University of Science and Technology (SUSTech), and the Special Funds for the Cultivation of Guangdong College Students' Scientific and Technological Innovation (pdjh2022c0003& pdjh2022c0005).

References:

[1] M. Green, E. Dunlop, J. Ebinger, M. Yoshita, N. Kopidakis, X. Hao. Progress in photovoltaics: research and applications, (2022) 1-14.

[2] H. Min, D.Y. Lee, J. Kim, G. Kim, K.S. Lee, J. Kim, M.J. Paik, Y.K. Kim, K.S. Kim, M.G. Kim, T.J. Shin, S. Il Seok, Nature, 598 (2021) 444-450.

[3] A. Kojima, K. Teshima, Y. Shirai, T. Miyasaka, J. Am. Chem. Soc.; 131 (2009) 6050-6051.

[4] B. Cai, Y. Xing, Z. Yang, W.-H. Zhang, J. Qiu, Energy & Environmental Science, 6 (2013) 1480-1485.

[5] L. Li, S. Zhang, Z. Yang, E.E.S. Berthold, W. Chen, Journal of Energy Chemistry, 27 (2018) 673-689.

[6] Z. Zhu, K. Mao, J. Xu, Journal of Energy Chemistry, 58 (2021) 219-232.

[7] J.Y. Jeng, K.C. Chen, T.Y. Chiang, P.Y. Lin, T.D. Tsai, Y.C. Chang, T.F. Guo, P. Chen, T.C. Wen, Y.J. Hsu, Adv Mater, 26 (2014) 4107-4113.

[8] Z. Zhu, Y. Bai, T. Zhang, Z. Liu, X. Long, Z. Wei, Z. Wang, L. Zhang, J. Wang, F. Yan, S. Yang, Angewandte Chemie, 126 (2014) 12779-12783.

[9] J. You, L. Meng, T.B. Song, T.F. Guo, Y.M. Yang, W.H. Chang, Z. Hong, H. Chen, H. Zhou, Q. Chen, Y. Liu, N. De Marco, Y. Yang, Nat Nanotechnol, 11 (2016) 75-81.

[10] G. Li, C.W. Chu, V. Shrotriya, J. Huang, Y. Yang, Applied Physics Letters, 88 (2006) 253503.

[11] V. Shrotriya, G. Li, Y. Yao, C.-W. Chu, Y. Yang, Applied Physics Letters, 88 (2006) 073508.

[12] X. Lin, D. Cui, X. Luo, C. Zhang, Q. Han, Y. Wang, L. Han, Energy & Environmental Science, 13 (2020) 3823-3847.

[13] F. Ma, Y. Zhao, J. Li, X. Zhang, H. Gu, J. You, Journal of Energy Chemistry, 52 (2021) 393-411.

[14] T. Liu, K. Chen, Q. Hu, R. Zhu, Q. Gong, Advanced Energy Materials, 6 (2016) 1600457.

[15] J.Y. Jeng, Y.F. Chiang, M.H. Lee, S.R. Peng, T.F. Guo, P. Chen, T.C. Wen, Adv Mater, 25 (2013) 3727-3732.

[16] D. Luo, W. Yang, Z. Wang, A. Sadhanala, Q. Hu, R. Su, R. Shivanna, G.F. Trindade, J.F. Watts, Z. Xu, T. Liu, K. Chen, F. Ye, P. Wu, L. Zhao, J. Wu, Y. Tu, Y. Zhang, X. Yang, W. Zhang, R.H. Friend, Q. Gong, H.J. Snaith, R. Zhu, Science, 360 (2018) 1442-1446.

[17] M. Stolterfoht, C.M. Wolff, J.A. Márquez, S. Zhang, C.J. Hages, D. Rothhardt, S. Albrecht, P.L. Burn, P. Meredith, T. Unold, D. Neher, Nature Energy, 3 (2018) 847-854.

[18] H. Chen, Q. Wei, M.I. Saidaminov, F. Wang, A. Johnston, Y. Hou, Z. Peng, K. Xu, W. Zhou, Z. Liu, L. Qiao, X. Wang, S. Xu, J. Li, R. Long, Y. Ke, E.H. Sargent, Z. Ning, Adv Mater, 31 (2019) e1903559.

[19] S. Yang, S. Chen, E. Mosconi, Y. Fang, X. Xiao, C. Wang, Y. Zhou, Z. Yu, J.

Zhao, Y. Gao, F. De Angelis, J. Huang, Science, 365 (2019) 473-478.

[20] S. Yang, J. Dai, Z. Yu, Y. Shao, Y. Zhou, X. Xiao, X.C. Zeng, J. Huang, J Am Chem Soc, 141 (2019) 5781-5787.

[21] F. Li, X. Deng, F. Qi, Z. Li, D. Liu, D. Shen, M. Qin, S. Wu, F. Lin, S.H. Jang, J. Zhang, X. Lu, D. Lei, C.S. Lee, Z. Zhu, A.K. Jen, J Am Chem Soc, 142 (2020) 20134-20142.

[22] P. Ru, E. Bi, Y. Zhang, Y. Wang, W. Kong, Y. Sha, W. Tang, P. Zhang, Y. Wu, W. Chen, X. Yang, H. Chen, L. Han, Advanced Energy Materials, 10 (2020) 1903487.

[23] K. Wang, C. Wu, Y. Hou, D. Yang, T. Ye, J. Yoon, M. Sanghadasa, S. Priya, Energy & Environmental Science, 13 (2020) 3412-3422.

[24] S. Wu, Z. Li, M.Q. Li, Y. Diao, F. Lin, T. Liu, J. Zhang, P. Tieu, W. Gao, F. Qi, X. Pan, Z. Xu, Z. Zhu, A.K. Jen, Nat Nanotechnol, 15 (2020) 934-940.

[25] S. Wu, J. Zhang, Z. Li, D. Liu, M. Qin, S.H. Cheung, X. Lu, D. Lei, S.K. So, Z. Zhu, A.K.Y. Jen, Joule, 4 (2020) 1248-1262.

[26] X. Zheng, Y. Hou, C. Bao, J. Yin, F. Yuan, Z. Huang, K. Song, J. Liu, J. Troughton, N. Gasparini, C. Zhou, Y. Lin, D.-J. Xue, B. Chen, A.K. Johnston, N. Wei, M.N. Hedhili, M. Wei, A.Y. Alsalloum, P. Maity, B. Turedi, C. Yang, D. Baran, T.D. Anthopoulos, Y. Han, Z.-H. Lu, O.F. Mohammed, F. Gao, E.H. Sargent, O.M. Bakr, Nature Energy, 5 (2020) 131-140.

[27] A.Y. Alsalloum, B. Turedi, K. Almasabi, X. Zheng, R. Naphade, S.D. Stranks, O.F. Mohammed, O.M. Bakr, Energy & Environmental Science, 14 (2021) 2263-2268.

[28] B. Chen, H. Chen, Y. Hou, J. Xu, S. Teale, K. Bertens, H. Chen, A. Proppe, Q. Zhou, D. Yu, K. Xu, M. Vafaie, Y. Liu, Y. Dong, E.H. Jung, C. Zheng, T. Zhu, Z. Ning, E.H. Sargent, Adv Mater, 33 (2021) e2103394.

[29] S. Chen, X. Dai, S. Xu, H. Jiao, L. Zhao, J. Huang, Science, 373 (2021) 902-907.

[30] S. Chen, X. Xiao, H. Gu, J. Huang, Sci Adv, 7 (2021) eabe8130.

[31] M. Degani, Q. An, M. Albaladejo-Siguan, Y.J. Hofstetter, C. Cho, F. Paulus, G. Grancini, Y. Vaynzof, Sci Adv, 7 (2021) eabj7930.

[32] S. Wu, Z. Li, J. Zhang, X. Wu, X. Deng, Y. Liu, J. Zhou, C. Zhi, X. Yu, W.C.H. Choy, Z. Zhu, A.K. Jen, Adv Mater, 33 (2021) e2105539.

[33] R. Azmi, E. Ugur, A. Seitkhan, F. Aljamaan, A.S. Subbiah, J. Liu, G.T. Harrison, M.I. Nugraha, M.K. Eswaran, M. Babics, Y. Chen, F. Xu, T.G. Allen, A.U. Rehman, C.L. Wang, T.D. Anthopoulos, U. Schwingenschlogl, M. De Bastiani, E. Aydin, S. De Wolf, Science, 376 (2022) eabm5784.

[34] X. Li, W. Zhang, X. Guo, C. Lu, J. Wei, J. Fang, Science, 375 (2022) 434-437.

[35] Z. Li, B. Li, X. Wu, S.A. Sheppard, S. Zhang, D. Gao, N.J. Long, Z. Zhu, Science, 376 (2022) 416-420.

[36] H. Chen, S. Teale, B. Chen, Y. Hou, L. Grater, T. Zhu, K. Bertens, S.M. Park, H.R. Atapattu, Y. Gao, M. Wei, A.K. Johnston, Q. Zhou, K. Xu, D. Yu, C. Han, T. Cui, E.H. Jung, C. Zhou, W. Zhou, A.H. Proppe, S. Hoogland, F. Laquai, T. Filleter, K.R.

Graham, Z. Ning, E.H. Sargent, Nature Photonics, 16 (2022) 352-358.

[37] Q. Jiang, J. Tong, Y. Xian, R.A. Kerner, S.P. Dunfield, C. Xiao, R.A. Scheidt, D. Kuciauskas, X. Wang, M.P. Hautzinger, R. Tirawat, M.C. Beard, D.P. Fenning, J.J. Berry, B.W. Larson, Y. Yan, K. Zhu, Nature, 611 (2022) 278–283.

[38] X. Zhou, L. Zhang, J. Yu, D. Wang, C. Liu, S. Chen, Y. Li, Y. Li, M. Zhang, Y. Peng, Y. Tian, J. Huang, X. Wang, X. Guo, B. Xu, Adv Mater, 34 (2022) e2205809.

[39] J. Wu, H. Cha, T. Du, Y. Dong, W. Xu, C.T. Lin, J.R. Durrant, Adv Mater, 34 (2022) e2101833.

[40] S. Tao, I. Schmidt, G. Brocks, J. Jiang, I. Tranca, K. Meerholz, S. Olthof, Nat Commun, 10 (2019) 2560.

[41] T. Minemoto, M. Murata, Solar Energy Materials and Solar Cells, 133 (2015) 8-14.

[42] Y. Raoui, H. Ez-Zahraouy, S. Kazim, S. Ahmad, Journal of Energy Chemistry, 54 (2021) 822-829.

[43] F. Gao, Y. Zhao, X. Zhang, J. You, Advanced Energy Materials, 10 (2019) 1902650.

[44] J.M. Ball, A. Petrozza, Nature Energy, 1 (2016) 1-13.

[45] C. Ran, J. Xu, W. Gao, C. Huang, S. Dou, Chem Soc Rev, 47 (2018) 4581-4610.

[46] B. Chen, P.N. Rudd, S. Yang, Y. Yuan, J. Huang, Chem Soc Rev, 48 (2019) 3842-3867.

[47] W. Shockley, W.T. Read, Physical Review, 87 (1952) 835-842.

[48] D. Xin, S. Tie, X. Zheng, J. Zhu, W.-H. Zhang, Journal of Energy Chemistry, 46 (2020) 173-177.

[49] D. Liu, D. Luo, A.N. Iqbal, K.W.P. Orr, T.A.S. Doherty, Z.H. Lu, S.D. Stranks, W. Zhang, Nat Mater, 20 (2021) 1337-1346.

[50] J. Wu, S.C. Liu, Z. Li, S. Wang, D.J. Xue, Y. Lin, J.S. Hu, Natl Sci Rev, 8 (2021) nwab047.

[51] C. Zhu, X. Niu, Y. Fu, N. Li, C. Hu, Y. Chen, X. He, G. Na, P. Liu, H. Zai, Y. Ge, Y. Lu, X. Ke, Y. Bai, S. Yang, P. Chen, Y. Li, M. Sui, L. Zhang, H. Zhou, Q. Chen, Nat Commun, 10 (2019) 815.

[52] Y. Chen, Y. Lei, Y. Li, Y. Yu, J. Cai, M.H. Chiu, R. Rao, Y. Gu, C. Wang, W. Choi, H. Hu, C. Wang, Y. Li, J. Song, J. Zhang, B. Qi, M. Lin, Z. Zhang, A.E. Islam, B. Maruyama, S. Dayeh, L.J. Li, K. Yang, Y.H. Lo, S. Xu, Nature, 577 (2020) 209-215.

[53] J. Zhao, Y. Deng, H. Wei, X. Zheng, Z. Yu, Y. Shao, J.E. Shield, J. Huang, Sci Adv, 3 (2017) eaao5616.

[54] K.A.B. Nicholas Rolston, Adam D. Printz, Aryeh Gold-Parker, Yichuan Ding, Michael F. Toney, Michael D. McGehee, and Reinhold H. Dauskardt*, Advanced Energy Materials, (2018) 1802139.

[55] H. Zhang, Z. Chen, M. Qin, Z. Ren, K. Liu, J. Huang, D. Shen, Z. Wu, Y. Zhang, J. Hao, C.S. Lee, X. Lu, Z. Zheng, W. Yu, G. Li, Adv Mater, 33 (2021) e2008487.

[56] S. Wang, J. Hu, A. Wang, Y. Cui, B. Chen, X. Niu, F. Hao, Journal of Energy

Chemistry, 66 (2022) 422-428.

[57] C. Bi, Q. Wang, Y. Shao, Y. Yuan, Z. Xiao, J. Huang, Nat Commun, 6 (2015) 7747.

[58] Z. Wan, H. Lai, S. Ren, R. He, Y. Jiang, J. Luo, Q. Chen, X. Hao, Y. Wang, J. Zhang, L. Wu, D. Zhao, Journal of Energy Chemistry, 57 (2021) 147-168.

[59] S. Ma, X. Zhang, X. Liu, R. Ghadari, M. Cai, Y. Ding, M. Mateen, S. Dai, Journal of Energy Chemistry, 54 (2021) 395-402.

[60] W.A. Dunlap-Shohl, Y. Zhou, N.P. Padture, D.B. Mitzi, Chem Rev, 119 (2019) 3193-3295.

[61] Z. Ni, C. Bao, Y. Liu, Q. Jiang, W.Q. Wu, S. Chen, X. Dai, B. Chen, B. Hartweg, Z. Yu, Z. Holman, J. Huang, Science, 367 (2020) 1352-1358.

[62] G. Tang, P. You, Q. Tai, A. Yang, J. Cao, F. Zheng, Z. Zhou, J. Zhao, P.K.L. Chan, F. Yan, Adv Mater, 31 (2019) e1807689.

[63] X. Liu, Y. Cheng, C. Liu, T. Zhang, N. Zhang, S. Zhang, J. Chen, Q. Xu, J. Ouyang, H. Gong, Energy & Environmental Science, 12 (2019) 1622-1633.

[64] Y. Huang, T. Liu, D. Li, Q. Lian, Y. Wang, G. Wang, G. Mi, Y. Zhou, A. Amini, B. Xu, Z. Tang, C. Cheng, G. Xing, Small, 18 (2022) e2201694.

[65] B. Li, Y. Xiang, K.D.G.I. Jayawardena, D. Luo, Z. Wang, X. Yang, J.F. Watts, S. Hinder, M.T. Sajjad, T. Webb, H. Luo, I. Marko, H. Li, S.A.J. Thomson, R. Zhu, G. Shao, S.J. Sweeney, S.R.P. Silva, W. Zhang, Nano Energy, 78 (2020) 105249.

[66] J. Wang, D. Li, Y. Luo, J. Wang, J. Peng, Advanced Materials Technologies, (2022) 2200370.

[67] S. Zhang, S.M. Hosseini, R. Gunder, A. Petsiuk, P. Caprioglio, C.M. Wolff, S. Shoaee, P. Meredith, S. Schorr, T. Unold, P.L. Burn, D. Neher, M. Stolterfoht, Adv Mater, 31 (2019) e1901090.

[68] C.M. Wolff, P. Caprioglio, M. Stolterfoht, D. Neher, Adv Mater, 31 (2019) e1902762.

[69] Q. Zhou, J. Qiu, Y. Wang, M. Yu, J. Liu, X. Zhang, ACS Energy Letters, (2021) 1596-1606.

[70] W. Yu, S. Ahmad, H. Zhang, Z. Chen, Q. Yang, X. Guo, C. Li, G. Li, Journal of Energy Chemistry, 56 (2021) 127-131.

[71] C. Wang, Q. Xiong, Z. Zhang, L. Meng, F. Li, L. Yang, X. Wang, Q. Zhou, W. Fan, L. Liang, S.Y. Lien, X. Li, J. Wu, P. Gao, ACS Appl Mater Interfaces, (2022) 12640-12651.

[72] X. Xu, X. Ji, R. Chen, F. Ye, S. Liu, S. Zhang, W. Chen, Y. Wu, W.H. Zhu, Advanced Functional Materials, 32 (2021) 2109968.

[73] S. Wang, Y. Li, J. Yang, T. Wang, B. Yang, Q. Cao, X. Pu, L. Etgar, J. Han, J. Zhao, X. Li, A. Hagfeldt, Angew Chem Int Ed Engl, 61 (2022) e202116534.

[74] Y. Chen, Z. Yang, S. Wang, X. Zheng, Y. Wu, N. Yuan, W.H. Zhang, S.F. Liu, Adv Mater, 30 (2018) e1805660.

[75] C. Yang, Z. Wang, Y. Lv, R. Yuan, Y. Wu, W.-H. Zhang, Chemical Engineering Journal, 406 (2021) 126855.

[76] Y. Chen, W. Tang, Y. Wu, X. Yu, J. Yang, Q. Ma, S. Wang, J. Jiang, S. Zhang, W.-H. Zhang, Chemical Engineering Journal, 425 (2021) 131499.

[77] A. Kotta, I. Seo, H.-S. Shin, H.-K. Seo, Chemical Engineering Journal, 435 (2022) 134805.

[78] R. Xu, X. Xu, R. Luo, Y. Li, G. Wang, T. Liu, N. Cai, S. Yang, Journal of Energy Chemistry, 67 (2022) 797-804.

[79] S. Zhang, X. Yan, Z. Liu, H. Zhu, Z. Yang, Y. Huang, S. Liu, D. Wu, M. Pan, W. Chen, Journal of Energy Chemistry, 54 (2021) 493-500.

[80] H. Bao, M. Du, H. Wang, K. Wang, X. Zuo, F. Liu, L. Liu, D. Eder, A. Cherevan, S. Wang, L. Wan, S. Zhao, S. Liu, Advanced Functional Materials, 31 (2021) 2102452.

[81] W. Chen, Y. Zhou, L. Wang, Y. Wu, B. Tu, B. Yu, F. Liu, H.W. Tam, G. Wang, A.B. Djurisic, L. Huang, Z. He, Adv Mater, 30 (2018) e1800515.

[82] W. Chen, Y.C. Zhou, G.C. Chen, Y.H. Wu, B. Tu, F.Z. Liu, L. Huang, A.M.C. Ng, A.B. Djurisic, Z.B. He, Advanced Energy Materials, 9 (2019) 1803872.

[83] J. Zhang, J. Long, Z. Huang, J. Yang, X. Li, R. Dai, W. Sheng, L. Tan, Y. Chen, Chemical Engineering Journal, 426 (2021) 131357.

[84] B. Zhang, J. Su, X. Guo, L. Zhou, Z. Lin, L. Feng, J. Zhang, J. Chang, Y. Hao, Adv Sci (Weinh), 7 (2020) 1903044.

[85] F. Sadegh, S. Akin, M. Moghadam, R. Keshavarzi, V. Mirkhani, M.A. Ruiz‐Preciado, E. Akman, H. Zhang, M. Amini, S. Tangestaninejad, I. Mohammadpoor‐Baltork, M. Graetzel, A. Hagfeldt, W. Tress, Advanced Functional Materials, 31 (2021) 2102237.

[86] Z. Liu, Q. Li, K. Chen, Y. Cui, J.J. Intemann, S. Leng, M. Cui, C. Qin, L. Fei, K. Yao, H. Huang, Journal of Materials Chemistry A, 9 (2021) 2394-2403.

[87] Y. Wang, H. Ju, T. Mahmoudi, C. Liu, C. Zhang, S. Wu, Y. Yang, Z. Wang, J. Hu, Y. Cao, F. Guo, Y.-B. Hahn, Y. Mai, Nano Energy, 88 (2021) 106285.

[88] Y. Chen, Z. Yang, X. Jia, Y. Wu, N. Yuan, J. Ding, W.-H. Zhang, S. Liu, Nano Energy, 61 (2019) 148-157.

[89] E. Yalcin, M. Can, C. Rodriguez-Seco, E. Aktas, R. Pudi, W. Cambarau, S. Demic, E. Palomares, Energy & Environmental Science, 12 (2019) 230-237.

[90] A. Magomedov, A. Al-Ashouri, E. Kasparavičius, S. Strazdaite, G. Niaura, M. Jošt, T. Malinauskas, S. Albrecht, V. Getautis, Advanced Energy Materials, 8 (2018) 1801892.

[91] L. Li, Y. Wang, X. Wang, R. Lin, X. Luo, Z. Liu, K. Zhou, S. Xiong, Q. Bao, G. Chen, Y. Tian, Y. Deng, K. Xiao, J. Wu, M.I. Saidaminov, H. Lin, C.-Q. Ma, Z. Zhao, Y. Wu, L. Zhang, H. Tan, Nature Energy, 7 (2022) 708-717.

[92] A. Al-Ashouri, A. Magomedov, M. Roß, M. Jošt, M. Talaikis, G. Chistiakova, T. Bertram, J.A. Márquez, E. Köhnen, E. Kasparavičius, S. Levcenco, L. Gil-Escrig, C.J. Hages, R. Schlatmann, B. Rech, T. Malinauskas, T. Unold, C.A. Kaufmann, L. Korte, G. Niaura, V. Getautis, S. Albrecht, Energy & Environmental Science, 12 (2019) 3356-3369.

[93] A. Al-Ashouri, E. Kohnen, B. Li, A. Magomedov, H. Hempel, P. Caprioglio, J.A. Marquez, A.B. Morales Vilches, E. Kasparavicius, J.A. Smith, N. Phung, D. Menzel, M. Grischek, L. Kegelmann, D. Skroblin, C. Gollwitzer, T. Malinauskas, M. Jost, G. Matic, B. Rech, R. Schlatmann, M. Topic, L. Korte, A. Abate, B. Stannowski, D. Neher, M. Stolterfoht, T. Unold, V. Getautis, S. Albrecht, Science, 370 (2020) 1300-1309.

[94] A. Ullah, K.H. Park, H.D. Nguyen, Y. Siddique, S.F.A. Shah, H. Tran, S. Park, S.I. Lee, K.K. Lee, C.H. Han, K. Kim, S. Ahn, I. Jeong, Y.S. Park, S. Hong, Advanced Energy Materials, 12 (2021) 2103175.

[95] A. Ullah, K.H. Park, Y. Lee, S. Park, A.B. Faheem, H.D. Nguyen, Y. Siddique, K.K. Lee, Y. Jo, C.H. Han, S. Ahn, I. Jeong, S. Cho, B. Kim, Y.S. Park, S. Hong, Advanced Functional Materials, (2022) 2208793.

[96] Z. Ren, K. Liu, H. Hu, X. Guo, Y. Gao, P.W.K. Fong, Q. Liang, H. Tang, J. Huang, H. Zhang, M. Qin, L. Cui, H.T. Chandran, D. Shen, M.F. Lo, A. Ng, C. Surya, M. Shao, C.S. Lee, X. Lu, F. Laquai, Y. Zhu, G. Li, Light Sci Appl, 10 (2021) 239.

[97] J.J. Yoo, G. Seo, M.R. Chua, T.G. Park, Y. Lu, F. Rotermund, Y.K. Kim, C.S. Moon, N.J. Jeon, J.P. Correa-Baena, V. Bulovic, S.S. Shin, M.G. Bawendi, J. Seo, Nature, 590 (2021) 587-593.

[98] J. Dou, Q. Song, Y. Ma, H. Wang, G. Yuan, X. Wei, X. Niu, S. Ma, X. Yang, J. Dou, S. Liu, H. Zhou, C. Zhu, Y. Chen, Y. Li, Y. Bai, Q. Chen, Journal of Energy Chemistry, 76 (2023) 288-294.

[99] X. Yang, D. Luo, Y. Xiang, L. Zhao, M. Anaya, Y. Shen, J. Wu, W. Yang, Y.H. Chiang, Y. Tu, R. Su, Q. Hu, H. Yu, G. Shao, W. Huang, T.P. Russell, Q. Gong, S.D. Stranks, W. Zhang, R. Zhu, Adv Mater, 33 (2021) e2006435.

[100] S. Chen, X. Xiao, B. Chen, L.L. Kelly, J. Zhao, Y. Lin, M.F. Toney, J. Huang, Sci Adv, 7 (2021) eabb2412.

[101] J. Li, L. Zuo, H. Wu, B. Niu, S. Shan, G. Wu, H. Chen, Advanced Functional Materials, 31 (2021) 2104036.

[102] Y. Chen, Y. shen, W. Tang, Y. Wu, W. Luo, N. Yuan, J. Ding, S. Zhang, W.H. Zhang, Advanced Functional Materials, 32 (2022) 2206703.

[103] Z. Zhu, K. Mao, K. Zhang, W. Peng, J. Zhang, H. Meng, S. Cheng, T. Li, H. Lin, Q. Chen, X. Wu, J. Xu, Joule, (2022).

[104] X. Li, G. Shen, X.R. Ng, Z. Liu, Y. Meng, Y.W. Zhang, C. Mu, Z.G. Yu, F. Lin, Energy & Environmental Materials, (2022) e12439.

[105] M. Du, S. Zhao, L. Duan, Y. Cao, H. Wang, Y. Sun, L. Wang, X. Zhu, J. Feng, L. Liu, X. Jiang, Q. Dong, Y. Shi, K. Wang, S. Liu, Joule, 6 (2022) 1931-1943.

[106] X. Hu, C. Zhu, W. Zhang, H. Wang, J. Wang, F. Ren, R. Chen, S. Liu, X. Meng, J. Zhou, Y. Pan, X. Tian, D. Sun, S. Zhang, Y. Zhang, Z. Liu, Q. Chen, W. Chen, Nano Energy, 101 (2022) 107594.

[107] R. Chen, S. Liu, X. Xu, F. Ren, J. Zhou, X. Tian, Z. Yang, X. Guanz, Z. Liu, S. Zhang, Y. Zhang, Y. Wu, L. Han, Y. Qi, W. Chen, Energy & Environmental Science, 15 (2022) 2567-2580.

[108] Q. Cao, J. Yang, T. Wang, Y. Li, X. Pu, J. Zhao, Y. Zhang, H. Zhou, X. Li, X. Li, Energy & Environmental Science, 14 (2021) 5406-5415.

[109] L. Xu, D. Wu, W. Lv, Y. Xiang, Y. Liu, Y. Tao, J. Yin, M. Qian, P. Li, L. Zhang, S. Chen, O.F. Mohammed, O.M. Bakr, Z. Duan, R. Chen, W. Huang, Adv Mater, 34 (2022) e2107111.

[110] F. Li, T.W. Lo, X. Deng, S. Li, Y. Fan, F.R. Lin, Y. Cheng, Z. Zhu, D. Lei, A.K.Y. Jen, Advanced Energy Materials, 12 (2022) 2200186.

[111] Y. Wu, N. Ding, Y. Zhang, B. Liu, X. Zhuang, S. Liu, Z. Nie, X. Bai, B. Dong, L. Xu, D. Zhou, H. Song, Advanced Energy Materials, 12 (2022) 2200005.

[112] Y.-N. Lu, J.-X. Zhong, Y. Yu, X. Chen, C.-Y. Yao, C. Zhang, M. Yang, W. Feng, Y. Jiang, Y. Tan, L. Gong, X. Wei, Y. Zhou, L. Wang, W.-Q. Wu, Energy & Environmental Science, 14 (2021) 4048-4058.

[113] Q. Cao, Y. Li, H. Zhang, J. Yang, J. Han, T. Xu, S. Wang, Z. Wang, B. Gao, J. Zhao, X. Li, X. Ma, S.M. Zakeeruddin, W.E.I. Sha, X. Li, M. Gratzel, Sci Adv, 7 (2021) eabg0633.

[114] X. Li, Y. Meng, R. Liu, Z. Yang, Y. Zeng, Y. Yi, W.E.I. Sha, Y. Long, J. Yang, Advanced Energy Materials, 11 (2021) 2102844.

[115] C. Chen, J. Liang, J. Zhang, X. Liu, X. Yin, H. Cui, H. Wang, C. Wang, Z. Li, J. Gong, Q. Lin, W. Ke, C. Tao, B. Da, Z. Ding, X. Xiao, G. Fang, Nano Energy, 90 (2021) 106608.

[116] F. Zhang, S. Ye, H. Zhang, F. Zhou, Y. Hao, H. Cai, J. Song, J. Qu, Nano Energy, 89 (2021) 106370.

[117] L. Zhou, J. Su, Z. Lin, X. Guo, J. Ma, T. Li, J. Zhang, J. Chang, Y. Hao, Research (Wash D C), 2021 (2021) 9836752.

[118] H. Hu, M. Qin, P.W.K. Fong, Z. Ren, X. Wan, M. Singh, C.J. Su, U.S. Jeng, L. Li, J. Zhu, M. Yuan, X. Lu, C.W. Chu, G. Li, Adv Mater, 33 (2021) e2006238.

[119] Y. Huang, T. Liu, B. Wang, J. Li, D. Li, G. Wang, Q. Lian, A. Amini, S. Chen, C. Cheng, G. Xing, Adv Mater, 33 (2021) e2102816.

[120] D. Li, W. Kong, H. Zhang, D. Wang, W. Li, C. Liu, H. Chen, W. Song, F. Gao, A. Amini, B. Xu, S. Li, C. Cheng, ACS Appl Mater Interfaces, 12 (2020) 20103-20109.

[121] L. Gao, J. You, S. Liu, Journal of Energy Chemistry, 57 (2021) 69-82.

[122] A.H. Proppe, A. Johnston, S. Teale, A. Mahata, R. Quintero-Bermudez, E.H. Jung, L. Grater, T. Cui, T. Filleter, C.Y. Kim, S.O. Kelley, F. De Angelis, E.H. Sargent, Nat Commun, 12 (2021) 3472.

[123] Y. Wang, J. Lin, Y. He, Y. Zhang, Q. Liang, F. Liu, Z. Zhou, C.C.S. Chan, G. Li, S.-P. Feng, A.M.C. Ng, K.S. Wong, J. Popović, A.B. Djurišić, Solar RRL, 6 (2022) 2200224.

[124] X. Liu, Z. Yu, T. Wang, K.L. Chiu, F. Lin, H. Gong, L. Ding, Y. Cheng, Advanced Energy Materials, 10 (2020) 2001958.

[125] S. Gharibzadeh, P. Fassl, I.M. Hossain, P. Rohrbeck, M. Frericks, M. Schmidt, T. Duong, M.R. Khan, T. Abzieher, B.A. Nejand, F. Schackmar, O. Almora, T.

Feeney, R. Singh, D. Fuchs, U. Lemmer, J.P. Hofmann, S.A.L. Weber, U.W. Paetzold, Energy & Environmental Science, 14 (2021) 5875-5893.

[126] W. Xu, Y. Gao, W. Ming, F. He, J. Li, X.H. Zhu, F. Kang, J. Li, G. Wei, Adv Mater, 32 (2020) e2003965.

[127] J. Yang, Q. Cao, Z. He, X. Pu, T. Li, B. Gao, X. Li, Nano Energy, 82 (2021) 105742.

[128] S. Wang, Z. He, J. Yang, T. Li, X. Pu, J. Han, Q. Cao, B. Gao, X. Li, Journal of Energy Chemistry, 60 (2021) 169-177.

[129] M. Zheng, Y. Miao, A.A. Syed, C. Chen, X. Yang, L. Ding, H. Li, M. Cheng, Journal of Energy Chemistry, 56 (2021) 374-382.

[130] W. Han, G. Ren, Z. Li, M. Dong, C. Liu, W. Guo, Journal of Energy Chemistry, 46 (2020) 202-207.

[131] A.D. Taylor, Q. Sun, K.P. Goetz, Q. An, T. Schramm, Y. Hofstetter, M. Litterst, F. Paulus, Y. Vaynzof, Nat Commun, 12 (2021) 1878.

[132] H. Sun, P. Dai, X. Li, J. Ning, S. Wang, Y. Qi, Journal of Energy Chemistry, 60 (2021) 300-333.

[133] C. Pereyra, H. Xie, M. Lira-Cantu, Journal of Energy Chemistry, 60 (2021) 599-634.

[134] S. Bai, P. Da, C. Li, Z. Wang, Z. Yuan, F. Fu, M. Kawecki, X. Liu, N. Sakai, J.T. Wang, S. Huettner, S. Buecheler, M. Fahlman, F. Gao, H.J. Snaith, Nature, 571 (2019) 245-250.

[135] K. Liu, Q. Liang, M. Qin, D. Shen, H. Yin, Z. Ren, Y. Zhang, H. Zhang, P.W.K. Fong, Z. Wu, J. Huang, J. Hao, Z. Zheng, S.K. So, C.-S. Lee, X. Lu, G. Li, Joule, 4 (2020) 2404-2425.

[136] T. Li, S. Wang, J. Yang, X. Pu, B. Gao, Z. He, Q. Cao, J. Han, X. Li, Nano Energy, 82 (2021) 105742.

[137] B. Niu, H. Wu, J. Yin, B. Wang, G. Wu, X. Kong, B. Yan, J. Yao, C.-Z. Li, H. Chen, ACS Energy Letters, 6 (2021) 3443-3449.

[138] S. Xiong, Z. Hou, S. Zou, X. Lu, J. Yang, T. Hao, Z. Zhou, J. Xu, Y. Zeng, W. Xiao, W. Dong, D. Li, X. Wang, Z. Hu, L. Sun, Y. Wu, X. Liu, L. Ding, Z. Sun, M. Fahlman, Q. Bao, Joule, 5 (2021) 467-480.

[139] Q. Yang, X. Liu, S. Yu, Z. Feng, L. Liang, W. Qin, Y. Wang, X. Hu, S. Chen, Z. Feng, G. Hou, K. Wu, X. Guo, C. Li, Energy & Environmental Science, 14 (2021) 6536-6545.

[140] M. Xiong, W. Zou, K. Fan, C. Qin, S. Li, L. Fei, J. Jiang, H. Huang, L. Shen, F. Gao, A.K.Y. Jen, K. Yao, ACS Energy Letters, 7 (2022) 550-559.

[141] Z. Zhou, H.J. Lian, J. Xie, W.C. Qiao, X.F. Wu, Y. Shi, X.L. Wang, S. Dai, H. Yuan, Y. Hou, S. Yang, H.G. Yang, Cell Reports Physical Science, 3 (2022) 100760.

[142] D. Li, Y. Huang, G. Wang, Q. Lian, R. Shi, L. Zhang, X. Wang, F. Gao, W. Kong, B. Xu, C. Cheng, S. Li, Journal of Materials Chemistry A, 9 (2021) 12746-12754.

[143] X. Deng, Z. Cao, C. Li, S. Wang, F. Hao, Journal of Energy Chemistry, 65 (2022) 592-599.

[144] J. Zhang, H. Yu, Journal of Energy Chemistry, 54 (2021) 291-300.

[145] F. Fan, Y. Zhang, M. Hao, F. Xin, Z. Zhou, Y. Zhou, Journal of Energy Chemistry, 68 (2022) 797-810.

[146] F. Wang, P. Wai-Keung Fong, Z. Ren, H.-L. Xia, K. Zhou, K. Wang, J. Zhu, X. Huang, X.-Y. Liu, H. Wang, Y. Shi, H. Lin, Q. Zhu, G. Li, H. Hu, Journal of Energy Chemistry, 73 (2022) 599-606.

[147] J. Yang, Y. Chen, W. Tang, S. Wang, Q. Ma, Y. Wu, N. Yuan, J. Ding, W.-H. Zhang, Journal of Energy Chemistry, 48 (2020) 217-225.

[148] T. Kong, H. Xie, Y. Zhang, J. Song, Y. Li, E.L. Lim, A. Hagfeldt, D. Bi, Advanced Energy Materials, 11 (2021) 2101018.

[149] G. Li, J. Song, J. Wu, Z. Song, X. Wang, W. Sun, L. Fan, J. Lin, M. Huang, Z. Lan, P. Gao, ACS Energy Letters, 6 (2021) 3614-3623.

[150] G. Wang, Q. Lian, D. Wang, F. Jiang, G. Mi, D. Li, Y. Huang, Y. Wang, X. Yao, R. Shi, C. Liao, J. Zheng, A. Ho-Baillie, A. Amini, B. Xu, C. Cheng, Adv Mater, 34 (2022) e2205143.

[151] Y. Ma, Q. Zhao, Journal of Energy Chemistry, 64 (2022) 538-560.

[152] S.-H. Bae, H. Zhao, Y.-T. Hsieh, L. Zuo, N. De Marco, You S. Rim, G. Li, Y. Yang, Chem, 1 (2016) 197-219.

[153] Q. Liang, K. Liu, M. Sun, Z. Ren, P.W.K. Fong, J. Huang, M. Qin, Z. Wu, D. Shen, C.S. Lee, J. Hao, X. Lu, B. Huang, G. Li, Adv Mater, 34 (2022) e2200276.

[154] K. Liu, P.W.K. Fong, Q. Liang, G. Li, Trends in Chemistry, 3 (2021) 747-764.

[155] P.W. Fong, H. Hu, Z. Ren, K. Liu, L. Cui, T. Bi, Q. Liang, Z. Wu, J. Hao, G. Li, Adv Sci (Weinh), 8 (2021) 2003359.

[156] M.A. Uddin, P.J.S. Rana, Z. Ni, X. Dai, Z. Yu, Z. Shi, H. Jiao, J. Huang, Adv Mater, 34 (2022) e2202954.

[157] D.X. Yuan, A. Gorka, M.F. Xu, Z.K. Wang, L.S. Liao, Phys Chem Chem Phys, 17 (2015) 19745-19750.

[158] F. Xie, C.-C. Chen, Y. Wu, X. Li, M. Cai, X. Liu, X. Yang, L. Han, Energy & Environmental Science, 10 (2017) 1942-1949.

[159] T. Du, T.J. Macdonald, R.X. Yang, M. Li, Z. Jiang, L. Mohan, W. Xu, Z. Su, X. Gao, R. Whiteley, C.T. Lin, G. Min, S.A. Haque, J.R. Durrant, K.A. Persson, M.A. McLachlan, J. Briscoe, Adv Mater, 34 (2022) e2107850.

[160] Y. Huang, T. Liu, D. Li, D. Zhao, A. Amini, C. Cheng, G. Xing, Nano Energy, 88 (2021) 106219.

[161] R. Wang, T. Huang, J. Xue, J. Tong, K. Zhu, Y. Yang, Nature Photonics, 15 (2021) 411-425.

[162] T. Leijtens, K.A. Bush, R. Prasanna, M.D. McGehee, Nature Energy, 3 (2018) 828-838.

[163] L. Tao, J. Qiu, B. Sun, X. Wang, X. Ran, L. Song, W. Shi, Q. Zhong, P. Li, H. Zhang, Y. Xia, P. Müller-Buschbaum, Y. Chen, Journal of Energy Chemistry, 61 (2021) 395-415.

[164] J. Liu, E. Aydin, J. Yin, M. De Bastiani, F.H. Isikgor, A.U. Rehman, E. Yengel, E. Ugur, G.T. Harrison, M. Wang, Y. Gao, J.I. Khan, M. Babics, T.G. Allen, A.S. Subbiah, K. Zhu, X. Zheng, W. Yan, F. Xu, M.F. Salvador, O.M. Bakr, T.D. Anthopoulos, M. Lanza, O.F. Mohammed, F. Laquai, S. De Wolf, Joule, 5 (2021) 3169-3186.

[165] K. Xiao, R. Lin, Q. Han, Y. Hou, Z. Qin, H.T. Nguyen, J. Wen, M. Wei, V. Yeddu, M.I. Saidaminov, Y. Gao, X. Luo, Y. Wang, H. Gao, C. Zhang, J. Xu, J. Zhu, E.H. Sargent, H. Tan, Nature Energy, 5 (2020) 870-880.

[166] K.A. Bush, K. Frohna, R. Prasanna, R.E. Beal, T. Leijtens, S.A. Swifter, M.D. McGehee, ACS Energy Letters, 3 (2018) 428-435.

[167] F.H. Isikgor, F. Furlan, J. Liu, E. Ugur, M.K. Eswaran, A.S. Subbiah, E. Yengel, M. De Bastiani, G.T. Harrison, S. Zhumagali, C.T. Howells, E. Aydin, M. Wang, N. Gasparini, T.G. Allen, A.u. Rehman, E. Van Kerschaver, D. Baran, I. McCulloch, T.D. Anthopoulos, U. Schwingenschlögl, F. Laquai, S. De Wolf, Joule, 5 (2021) 1566-1586.

[168] S. Qin, C. Lu, Z. Jia, Y. Wang, S. Li, W. Lai, P. Shi, R. Wang, C. Zhu, J. Du, J. Zhang, L. Meng, Y. Li, Adv Mater, 34 (2022) e2108829.

[169] X. Zheng, B. Chen, J. Dai, Y. Fang, Y. Bai, Y. Lin, H. Wei, Xiao C. Zeng, J. Huang, Nature Energy, 2 (2017) 1-9.

[170] M. De Bastiani, A.J. Mirabelli, Y. Hou, F. Gota, E. Aydin, T.G. Allen, J. Troughton, A.S. Subbiah, F.H. Isikgor, J. Liu, L. Xu, B. Chen, E. Van Kerschaver, D. Baran, B. Fraboni, M.F. Salvador, U.W. Paetzold, E.H. Sargent, S. De Wolf, Nature Energy, 6 (2021) 167-175.

[171] D. Kim, H.J. Jung, I.J. Park, B.W. Larson, S.P. Dunfield, C. Xiao, J. Kim, J. Tong, P. Boonmongkolras, S.G. Ji, F. Zhang, S.R. Pae, M. Kim, S.B. Kang, V. Dravid, J.J. Berry, J.Y. Kim, K. Zhu, D.H. Kim, B. Shin, Science, 368 (2020) 155-160.

[172] S. Chen, Y. Hou, H. Chen, M. Richter, F. Guo, S. Kahmann, X. Tang, T. Stubhan, H. Zhang, N. Li, N. Gasparini, C.O.R. Quiroz, L.S. Khanzada, G.J. Matt, A. Osvet, C.J. Brabec, Advanced Energy Materials, 6 (2016) 1600132.

[173] J. Tao, X. Liu, J. Shen, S. Han, L. Guan, G. Fu, D.B. Kuang, S. Yang, ACS Nano, (2022) 10798-10810.

[174] S. Singh, D. Kabra, Journal of Materials Chemistry C, 6 (2018) 12052-12061.

[175] W. Chen, Y. Zhu, J. Xiu, G. Chen, H. Liang, S. Liu, H. Xue, E. Birgersson, J.W. Ho, X. Qin, J. Lin, R. Ma, T. Liu, Y. He, A.M.-C. Ng, X. Guo, Z. He, H. Yan, A.B. Djurišić, Y. Hou, Nature Energy, 7 (2022) 229-237.

[176] Y.H. Lin, N. Sakai, P. Da, J. Wu, H.C. Sansom, A.J. Ramadan, S. Mahesh, J. Liu, R.D.J. Oliver, J. Lim, L. Aspitarte, K. Sharma, P.K. Madhu, A.B. Morales-Vilches, P.K. Nayak, S. Bai, F. Gao, C.R.M. Grovenor, M.B. Johnston, J.G. Labram, J.R. Durrant, J.M. Ball, B. Wenger, B. Stannowski, H.J. Snaith, Science, 369 (2020) 96-102.

[177] M. Hu, C. Bi, Y. Yuan, Y. Bai, J. Huang, Adv Sci (Weinh), 3 (2016) 1500301.

[178] J. Liang, C. Chen, X. Hu, Z. Chen, X. Zheng, J. Li, H. Wang, F. Ye, M. Xiao, Z. Lu, Y. Xu, S. Zhang, R. Yu, C. Tao, G. Fang, ACS Appl Mater Interfaces, 12 (2020)

48458-48466.

[179] R.D.J. Oliver, P. Caprioglio, F. Peña-Camargo, L.R.V. Buizza, F. Zu, A.J. Ramadan, S.G. Motti, S. Mahesh, M.M. McCarthy, J.H. Warby, Y.-H. Lin, N. Koch, S. Albrecht, L.M. Herz, M.B. Johnston, D. Neher, M. Stolterfoht, H.J. Snaith, Energy & Environmental Science, 15 (2022) 714-726.

[180] L. Kuai, Y. Wang, Z. Zhang, Y. Yang, Y. Qin, T. Wu, Y. Li, Y. Li, T. Song, X. Gao, L. Wang, B. Sun, Solar RRL, 3 (2019) 1900053.

[181] L. Wang, G. Wang, Z. Yan, J. Qiu, C. Jia, W. Zhang, C. Zhen, C. Xu, K. Tai, X. Jiang, S. Yang, Solar RRL, 4 (2020) 2000098.

[182] C. Wang, W. Shao, J. Liang, C. Chen, X. Hu, H. Cui, C. Liu, G. Fang, C. Tao, Small, (2022) e2204081.

[183] K. Dey, B. Roose, S.D. Stranks, Adv Mater, 33 (2021) e2102300.

[184] Z. Jin, B.-B. Yu, M. Liao, D. Liu, J. Xiu, Z. Zhang, E. Lifshitz, J. Tang, H. Song, Z. He, Journal of Energy Chemistry, 54 (2021) 414-421.

[185] S. Gu, R. Lin, Q. Han, Y. Gao, H. Tan, J. Zhu, Adv Mater, 32 (2020) e1907392.

[186] Z. Fang, Q. Zeng, C. Zuo, L. Zhang, H. Xiao, M. Cheng, F. Hao, Q. Bao, L. Zhang, Y. Yuan, W.-Q. Wu, D. Zhao, Y. Cheng, H. Tan, Z. Xiao, S. Yang, F. Liu, Z. Jin, J. Yan, L. Ding, Science Bulletin, 66 (2021) 621-636.

[187] R. Lin, J. Xu, M. Wei, Y. Wang, Z. Qin, Z. Liu, J. Wu, K. Xiao, B. Chen, S.M. Park, G. Chen, H.R. Atapattu, K.R. Graham, J. Xu, J. Zhu, L. Li, C. Zhang, E.H. Sargent, H. Tan, Nature, 603 (2022) 73-78.

[188] J. Tong, Z. Song, D.H. Kim, X. Chen, C. Chen, A.F. Palmstrom, P.F. Ndione, M.O. Reese, S.P. Dunfield, O.G. Reid, J. Liu, F. Zhang, S.P. Harvey, Z. Li, S.T. Christensen, G. Teeter, D. Zhao, M.M. Al-Jassim, M. van Hest, M.C. Beard, S.E. Shaheen, J.J. Berry, Y. Yan, K. Zhu, Science, 364 (2019) 475-479.

[189] H. Hu, Xianyong, J. Chen, D. Wang, D. Li, Y. Huang, L. Zhang, Y. Peng, F. Wang, J. Huang, N. Chen, L. Sun, X. Liu, X. Wang, J. Ouyang, B. Xu, Energy & Environmental Materials, 0 (2022) 1-7.

[190] Z. Yu, X. Chen, S.P. Harvey, Z. Ni, B. Chen, S. Chen, C. Yao, X. Xiao, S. Xu, G. Yang, Y. Yan, J.J. Berry, M.C. Beard, J. Huang, Adv Mater, 34 (2022) e2110351.

[191] X. Zhou, L. Zhang, X. Wang, C. Liu, S. Chen, M. Zhang, X. Li, W. Yi, B. Xu, Adv Mater, 32 (2020) e1908107.

[192] H. Kim, J.W. Lee, G.R. Han, Y.J. Kim, S.H. Kim, S.K. Kim, S.K. Kwak, J.H. Oh, Advanced Functional Materials, 32 (2021) 2110069.

[193] J. Tong, J. Gong, M. Hu, S.K. Yadavalli, Z. Dai, F. Zhang, C. Xiao, J. Hao, M. Yang, M.A. Anderson, E.L. Ratcliff, J.J. Berry, N.P. Padture, Y. Zhou, K. Zhu, Matter, 4 (2021) 1365-1376.

[194] J. Cao, H.L. Loi, Y. Xu, X. Guo, N. Wang, C.K. Liu, T. Wang, H. Cheng, Y. Zhu, M.G. Li, W.Y. Wong, F. Yan, Adv Mater, 34 (2022) e2107729.

[195] W. Zhang, X. Li, S. Fu, X. Zhao, X. Feng, J. Fang, Joule, 5 (2021) 2904-2914.

[196] D. Zhao, Y. Yu, C. Wang, W. Liao, N. Shrestha, C.R. Grice, A.J. Cimaroli, L. Guan, R.J. Ellingson, K. Zhu, X. Zhao, R.-G. Xiong, Y. Yan, Nature Energy, 2 (2017) 1-7.

[197] H. Liu, L. Wang, R. Li, B. Shi, P. Wang, Y. Zhao, X. Zhang, ACS Energy Letters, 6 (2021) 2907-2916.

[198] R. Lin, K. Xiao, Z. Qin, Q. Han, C. Zhang, M. Wei, M.I. Saidaminov, Y. Gao, J. Xu, M. Xiao, A. Li, J. Zhu, E.H. Sargent, H. Tan, Nature Energy, 4 (2019) 864-873.

[199] D. Yu, Q. Wei, H. Li, J. Xie, X. Jiang, T. Pan, H. Wang, M. Pan, W. Zhou, W. Liu, P.C.Y. Chow, Z. Ning, Angew Chem Int Ed Engl, 61 (2022) e202202346.

[200] Z. Liang, H. Xu, Y. Zhang, G. Liu, S. Chu, Y. Tao, X. Xu, S. Xu, L. Zhang, X. Chen, B. Xu, Z. Xiao, X. Pan, J. Ye, Adv Mater, 34 (2022) e2110241.

[201] G. Kapil, T. Bessho, T. Maekawa, A.K. Baranwal, Y. Zhang, M.A. Kamarudin, D. Hirotani, Q. Shen, H. Segawa, S. Hayase, Advanced Energy Materials, 11 (2021) 2101069.

[202] G. Kapil, T. Bessho, Y. Sanehira, S.R. Sahamir, M. Chen, A.K. Baranwal, D. Liu, Y. Sono, D. Hirotani, D. Nomura, K. Nishimura, M.A. Kamarudin, Q. Shen, H. Segawa, S. Hayase, ACS Energy Letters, 7 (2022) 966-974.

[203] Y.-M. Xie, T. Niu, Q. Yao, Q. Xue, Z. Zeng, Y. Cheng, H.-L. Yip, Y. Cao, Journal of Energy Chemistry, 71 (2022) 12-19.

[204] W. Cao, Z. Hu, Z. Lin, X. Guo, J. Su, J. Chang, Y. Hao, Journal of Energy Chemistry, 68 (2022) 420-438.

[205] W. Liao, D. Zhao, Y. Yu, C.R. Grice, C. Wang, A.J. Cimaroli, P. Schulz, W. Meng, K. Zhu, R.G. Xiong, Y. Yan, Adv Mater, 28 (2016) 9333-9340.

[206] Z. Chen, M. Liu, Z. Li, T. Shi, Y. Yang, H.L. Yip, Y. Cao, iScience, 9 (2018) 337-346.

[207] S. Hu, K. Otsuka, R. Murdey, T. Nakamura, M.A. Truong, T. Yamada, T. Handa, K. Matsuda, K. Nakano, A. Sato, K. Marumoto, K. Tajima, Y. Kanemitsu, A. Wakamiya, Energy & Environmental Science, 15 (2022) 2096-2107.

[208] Z. Zhang, J. Liang, Y. Zheng, X. Wu, J. Wang, Y. Huang, Y. Yang, Z. Zhou, L. Wang, L. Kong, K.M. Reddy, C. Qin, C.-C. Chen, Journal of Materials Chemistry A, 9 (2021) 17830-17840.

[209] W. Chen, H. Sun, Q. Hu, A.B. Djurišić, T.P. Russell, X. Guo, Z. He, ACS Energy Letters, 4 (2019) 2535-2536.

[210] Q. Hu, W. Chen, W. Yang, Y. Li, Y. Zhou, B.W. Larson, J.C. Johnson, Y.-H. Lu, W. Zhong, J. Xu, L. Klivansky, C. Wang, M. Salmeron, A.B. Djurišić, F. Liu, Z. He, R. Zhu, T.P. Russell, Joule, 4 (2020) 1575-1593.

[211] K.O. Brinkmann, T. Becker, F. Zimmermann, C. Kreusel, T. Gahlmann, M. Theisen, T. Haeger, S. Olthof, C. Tuckmantel, M. Gunster, T. Maschwitz, F. Gobelsmann, C. Koch, D. Hertel, P. Caprioglio, F. Pena-Camargo, L. Perdigon-Toro, A. Al-Ashouri, L. Merten, A. Hinderhofer, L. Gomell, S. Zhang, F. Schreiber, S. Albrecht, K. Meerholz, D. Neher, M. Stolterfoht, T. Riedl, Nature, 604 (2022) 280-286.

Graphic abstract

Inverted perovskite solar cells (IPSCs) show great promise in commercialization due to easy fabrication, good stability, and wide application. This review summarized challenges and solutions in IPSCs and guided their development direction.